---

**Article:**
Brown, L.M., Thornton, S.F. and Baú, D. (2024) Enhancing in situ biodegradation in groundwater using pump and treat remediation: a proof of concept and modelling analysis of controlling variables. Environmental Science and Pollution Research. ISSN 1614-7499

https://doi.org/10.1007/s11356-024-32662-x

---

# Enhancing *in situ* biodegradation in groundwater using pump and treat remediation: a proof of concept and modelling analysis of controlling variables.

Luther M. Brown[1*], Steven F. Thornton[1], Domenico Baú[1]

## Abstract

A remediation approach which uses pump and treatment (PAT) to enhance the biodegradation of organic contaminants by increasing dispersive mixing between plumes and groundwater was evaluated for a phenol-contaminated aquifer, using a reactive transport model which simulates kinetic reactions between an electron donor (ED) in the plume and electron acceptor (EA) in the groundwater. The influence of system design and operation was examined in six modelling scenarios. Injection or extraction of groundwater increases biodegradation above no action and the location, pumping rate and distance between well(s) are important variables which influence biodegradation. An increase in pumping rate, distance of the wells from the plume centreline and changing the flow direction increases dispersive mixing between the plume and groundwater. This increases plume spreading and the plume fringe interface, providing a greater flux of dissolved EAs for biodegradation. In general, injection of groundwater containing natural EAs enhances biodegradation more than extraction. The enhancement of biodegradation is sensitive to the relative fluxes of ED and EA, as controlled by the arrangement of the wells. In the best performing scenario, biodegradation was enhanced by 128%, compared with no action.

Keywords: phenol, groundwater, biodegradation, remediation, natural attenuation, pump and treat

---

[1] Groundwater Protection and Restoration Group, Civil and Structural Engineering, University of Sheffield, Mappin Street, Sheffield, S1 3JD, UK. Email: lmbrown1@sheffield.ac.uk. Tel: +44 114 222 0253.

*To whom correspondence should be addressed

## Acknowledgements

The authors thank Vivek Bedekar (SS Papadopulos and Associates, Inc.) for helpful discussions on the use of MT3D-USGS in the model development and scenario analysis. Three anonymous reviewers are thanked for their thoughtful and insightful comments, which helped improve the manuscript.

## 1. Introduction

Groundwater contamination by organic compounds is a major global problem, with at least 300,000 sites in the U.S. alone requiring remediation at an estimated cost of US$ 127B (NRC, 2013). There are a comparable number of contaminated sites in Europe that require remediation (Antelmi et al., 2020). A significant number of sites are unlikely to reach remediation targets within 50-100 years. For example, pump and treat (PAT) systems installed at US Superfund sites in the 1990s are still operating today, with current systems expected to have comparable operational timescales (USEPA, 2021).

PAT is most often used for hydraulic manipulation of contaminant plumes (source control/reduction and plume containment to prevent expansion or offsite migration), to reduce contaminant concentrations *in situ*, or to remove dissolved and mobile free-phase contaminant mass in groundwater for treatment (Mackay and Cherry, 1989; USEPA, 1990; 1996; Cohen et al., 1997; Suthersan et al., 2015; Truex et al., 2017; Speight, 2020). PAT is used to treat a wide range of contaminants, including coal tar distillates, phenols, polycyclic aromatic hydrocarbons, heterocyclic aromatic compounds, fuel hydrocarbons, and chlorinated solvents (Truex et al., 2017; Speight, 2020), and is most effective for the removal of contaminants in alluvial aquifers with relatively homogenous hydrogeological properties (USEPA, 1990; 1996; NRC, 2013). The limitations of PAT are well known and in more complex aquifers contaminant sorption-desorption hysteresis, free-phase dissolution kinetics and/or matrix diffusion may affect the effectiveness and application of this technology (Keely, 1989; USEPA, 1990; 1996; Cohen et al., 1997; McDade et al., 2013; NRC, 2013; Truex et al., 2017; Guo et al., 2019; Speight, 2020). Consequently, PAT systems are often used in combination with other remediation techniques to achieve clean-up goals at contaminated sites (USEPA, 1990; 1996; Cohen et al., 1997; Bayer et al., 2004; CRC CARE, 2019).

Natural attenuation (NA) is a risk-based remediation method, wherein the combined effect of naturally occurring physical, chemical and biological processes are used to treat contaminants *in situ* (Wiedemeier et al., 1999). Biodegradation is typically the most important process for organic contaminant attenuation (Bauer et al., 2009; Meckenstock et al., 2015). In contaminated groundwater, the plume fringe is a zone of enhanced biodegradation activity at the interface between the background groundwater and contaminant plume, driven by the dispersive mixing of electron acceptors (EA) in groundwater with biodegradable organic compounds in the plume (Thornton et al., 2001a,b; 2014; Jones et al., 2002; Tuxen et al., 2006; Bauer et al., 2009). As the length scale of dispersion is small relative to the size of a contaminant plume, reactions are limited to a narrow region at the plume fringe where the substrate and EAs mix (Reising, 2018; Sather et al., 2022; 2023). Biodegradation in plumes is limited

by dissolved EA availability and aquifer dispersivity (Cirpka et al., 1999; Lerner et al., 2000; Thornton et al., 2001a; Jones et al., 2002; Tuxen et al., 2006; Sather et al., 2022; 2023), but can be increased if the supply (i.e. mass flux) of EAs into the plume can be increased by promoting mixing of the background groundwater and plume. Solute mixing in porous media can be enhanced by increasing the magnitude of dispersion, principally by controlling the flow velocity (Bagtzoglou and Oates, 2007; Werth et al., 2006; Ye et al., 2015; Neupauer et al., 2020). Furthermore, dispersive mixing of reactants can occur due to anisotropy, hydraulic conductivity contrasts between porous media, chaotic advection, flow-folding and flow focusing in high permeability zones (Bagtzoglou and Oates, 2007; Werth et al., 2006; Eckert et al., 2012; Piscopo et al., 2013; Ye et al., 2015; 2021; Xu et al., 2018; Suk et al., 2021; Sather et al., 2023). Consequently, biodegradation can be increased under conditions which enhance the flow velocity and/or dispersion (Werth et al., 2006; Bauer et al., 2009). Hence, the PAT system may be used to address mass transport limits on *in situ* biodegradation, by suitable modification of the ambient flow field to enhance dispersive mixing of solutes.

Previously, Thornton et al. (2014) demonstrated at the field scale that the biodegradation of phenolic compounds can be increased by a PAT well pumping at the plume fringe. In that study, the *in situ* biodegradation rate of phenolic compounds at the plume fringe doubled over a 3-year period during operation of the PAT (groundwater extraction rate of 6-50 $m^3$/d). This was achieved by reducing the concentration of phenolic compounds in the plume which inhibit biodegradation (dilution of plume contaminants) and increasing the dispersive mass flux of dissolved EAs into the plume from the background groundwater (induced by the elevated pumping rates) and surface area of the plume fringe interface for biodegradation. This study therefore showed that it is possible to combine PAT with NA to improve remediation performance, by suitable modification of the ambient flow field to enhance dispersive mixing of solutes, although this is logically influenced by the design of the PAT system (e.g. injection/extraction well locations and spacing, pumping rate and duration).

Given the limitations of conventional PAT systems, the integration of these with other remediation techniques is recommended to enhance its effectiveness (USEPA, 1990; 1996; 2021). However, while guidelines exist for the deployment of conventional PAT systems (e.g. Cohen et al, 1997; USEPA, 1990; 1996; 2021), there is currently no technical basis to support the development of an integrated PAT and NA system (as proposed herein) for contaminated groundwater remediation. The motivation for this research is to explore the scientific basis for integrating PAT with NA as a remediation concept. The novelty of the study lies in the synergy of combining the two technical approaches of PAT with NA to increase mass biodegradation relative to mass extraction by the PAT

well(s), over that possible with PAT alone. While well location, pumping rate and injection/extraction strategies are known to influence remediation performance in these separate contexts, this has not been formally considered in their combined application. The aim of this study is therefore to examine this approach as a proof of concept and to understand the influence of operational variables, such as well location, pumping strategy and rate, on PAT performance to enhance the *in situ* biodegradation of organic contaminants in groundwater for remediation and plume management. The specific objectives are to:

(a) Analyze the effect of well location, pumping rate and pumping strategy on mass removal and biodegradation;

(b Identify strategies which increase the mass biodegraded relative to the total contaminant mass extracted; and

(c) Investigate the effectiveness of a PAT system that combines extraction and injection of groundwater.

The approach is evaluated at a site on a UK sandstone aquifer contaminated with a plume of phenolic compounds, in which a PAT system has been installed for plume management (Baker et al., 2012; Thornton et al., 2014). Phenol is a common groundwater contaminant from many industrial processes (e.g. wood preservation plants, organic chemical manufacturing, coal tar processing, gasworks) and is used as a candidate organic contaminant in this study.

## 2. Theoretical and conceptual considerations relating to plume fringe development

Biodegradation processes are characteristically spatially distributed in organic contaminant plumes (Gutierrez-Neri et al., 2009; Thornton, 2019; van Leeuwen et al., 2022) and the presence of a bioreactive fringe in groundwater plumes has been known for decades (Dakins et al., 1996; Schmieman et al., 1997). In recent years the plume fringe vs plume core concept has been proposed to explain biodegradation in contaminant plumes (Prommer et al., 2006; Meckenstock et al., 2015; McLeod et al., 2018), complementing the classical conceptual model of longitudinal redox zonation (e.g. Chapelle, 2000; Christensen et al., 2000; Cribbin et al., 2014).

The plume fringe is a dynamic interface between the background groundwater and plume, marked by large solute counter concentration gradients which promote transverse dispersion and mixing between electron donors (e.g. organic contaminants) and dissolved electron acceptors (e.g. $O_2$ and $NO_3$) in these chemically different waters. The gradients in geochemical species influence the microbial community composition and distribution of microorganisms across the plume fringe, which in turn can determine the potential for biodegradation of specific contaminants in groundwater (Tuxen et al., 2006; Winderl et al., 2008; Prommer et al., 2009; Anneser et al., 2010; Brad et al., 2013; Rizoulis et al., 2013; Larentis et al., 2013; Pilloni et al., 2019). This feature has been

demonstrated in many field and modelling studies (e.g. Lerner et al., 2000; Mayer et al., 2001; Thornton et al., 2001b, 2014; van Breukelen and Griffioen, 2004; Chu et al., 2005; Watson et al., 2005; Prommer et al., 2006, 2009; Maier et al., 2007; Anneser et al., 2008; Cribbins et al., 2014; McLeod et al., 2018) and is a zone of significantly increased microbial activity (Tuxen et al., 2006; Jobelius et al., 2011; Brad et al., 2013; Rizoulis et al., 2013; Fahrenfeld et al., 2014; Eckert et al., 2015) relative to other locations in plumes.

Conversely, anaerobic biodegradation in the plume core, which includes methanogenesis and respiratory processes using Mn, Fe, and $SO_4$ as EAs, is generally less important for contaminant mass removal than biodegradation at the plume fringe (Meckenstock et al., 2015; Thornton, 2019). In stationary plumes, this occurs due to depletion of dissolved EAs at the source, ongoing microbial activity and energetically slower reaction rates for these processes in the plume core (Cribbins et al., 2014; Eckert et al., 2015; Meckenstock et al., 2015; van Leeuwen et al., 2022). While the plume fringe is characteristically very narrow (e.g. < 1 m, and dependent on sampling resolution), it is a zone of enhanced biodegradation and biotransformation for many contaminants, including phenols (Lerner et al, 2000; Pickup et al., 2001; Thornton et al., 2001a; Baker et al., 2012; Rizoulis et al., 2013), gasoline hydrocarbons and oxygenate compounds (Day and Gulliver, 2003; Spence et al., 2005; Thornton et al., 2011), phenoxy acid herbicides (Prommer et al., 2006; Tuxen et al., 2006), (poly)aromatic hydrocarbons and tar oil compounds (Prommer et al., 2009; Anneser et al., 2010; Amos et al., 2011; Pilloni et al., 2019; van Leeuwen et al., 2022), NSO-heterocyclic compounds (Salowsky et al., 2012), chlorinated compounds (Olaniran et al., 2008), nutrients (Lorah et al., 2009), ethanol (McLeod et al., 2018) and metals (Schmieman et al., 1997). Furthermore, the cycling of redox species between dissolved and mineral-based forms at the plume fringe, involving both biologically catalysed and abiotic reactions, is an important process influencing the fate of many organic and inorganic contaminants in groundwater plumes (Spence et al., 2001; Topinkova et al., 2007; Vencelides et al., 2007; Einsiedl et al., 2015).

The development of the plume fringe is strongly affected by spatio-temporal variation in the local velocity field, which influences the extent of dispersive mixing and plume spreading. Mixing is controlled by molecular diffusion and small (pore)-scale hydrodynamic dispersion, which results in the smoothing of solute concentration gradients across the plume fringe interface (Piscopo et al., 2013; Neupauer et al., 2020). Mixing of contaminants and EAs by transverse dispersion is rate limiting for overall biodegradation in steady-state plumes (Cirpka et al., 1999, 2006; Chu et al., 2005; Cribbins et al., 2014; Eckert et al., 2012, 2015; Meckenstock et al., 2015; Xu et al., 2018). Spreading involves reconfiguration of the plume geometry by both passive and active mechanisms. Passive

spreading (manifested as macrodispersion) results from variation in natural flow velocity caused by heterogeneity in the aquifer hydraulic conductivity distribution (Cirpka et al., 2006). Conversely, active spreading results from variation in the velocity field induced by unsteady flows created by pumping, for example engineered injection and extraction (Piscopo et al., 2013; Neupauer et al., 2020). Spreading the plume promotes mixing by increasing the solute concentration gradients and contact area between the compositionally different waters at the interface, both of which increase mass flux by diffusion (Cirpka et al., 2006; Piscopo et al., 2013; Ye et al., 2021; Sather et al., 2022). Importantly, active spreading enhances mixing and reaction through both longitudinal and transverse dispersion (Sather et al., 2023). However, while longitudinal dispersion in the direction of groundwater flow is an important mixing process and is higher in magnitude than transverse horizontal and vertical dispersion, mixing due to local-scale transverse dispersion may control the reactive behaviour of interacting compounds on the aquifer-scale (Cirpka et al., 1999, 2006; Ye et al., 2015; Neupauer et al., 2020). In general, steady-state plume lengths are inversely correlated with aquifer bulk transverse dispersivity, but transverse mixing at the plume fringe can successfully constrain plume migration (Cirpka et al., 2006; Chu et al., 2005).

## 3 Methodology

### 3.1 Study site

The considered field site is a fine-grained, unconfined, fluviatile, sandstone bedrock aquifer located underneath a former coal tar distillation plant in UK. The site has been extensively investigated over 25 years, with studies on the interpretation of groundwater contamination (Williams et al., 2001), redox processes and contaminant biodegradation (Thornton et al., 2001a; 2014; Wu et al., 2006; Baker et al., 2012;), aquifer stable isotope geochemistry (Spence et al., 2001), aquifer microbiology (Pickup et al., 2001; Elliot et al., 2010; Rizoulis et al., 2013; Mujica-Alarcon et al., 2021), plume mass balance (Thornton et al., 2001b) and reactive transport modelling (Mayer et al., 2001; Watson et al., 2005). The site history, summarised here, is described in detail in Williams et al. (2001).

A mixed plume of phenolic compounds (primarily phenol, cresols and xylenols) extends approximately 700 m down hydraulic gradient of the site, with an estimated width of 150 m and depth of 60 m. Groundwater flow is westerly, with a pore velocity between 4-11 m/year, consistent over the history of the plume. Vertical flow due to groundwater recharge is also important (Table 1). Previous investigations have identified a heterogeneous distribution of phenolic compounds and biogeochemical processes responsible for their biodegradation within the plume (Thornton et al, 2001a). The plume is anchored by a dense non-aqueous phase liquid (DNAPL) source,

with concentrations of individual phenolic compounds (e.g., phenol) reaching 25,000 mg/l. Considering this, and to reduce the complexity of the numerical model, phenol was selected as a representative organic contaminant for the simulations and the concentrations of all other phenolic compounds were converted into equivalent phenol concentrations.

Previous studies have shown that the phenolic contaminants are biodegraded by several processes, with most mass loss (>90%) arising from consumption of oxygen and nitrate in the groundwater (Lerner et al., 2000; Thornton et al., 2001a,b; Mayer et al., 2001; Jones et al., 2002; Watson et al., 2005). For this reason, the modelling scenarios were developed to assess the contribution of these two EAs to biodegradation, as influenced by the PAT system.

### 3.2 Flow and reactive transport model

A 3-D flow and transport model was developed using the input data in Table 1. Groundwater flow is governed by the classical PDE:

$$\frac{\partial}{\partial x}\left(K_{xx}\frac{\partial h}{\partial x}\right)+\frac{\partial}{\partial y}\left(K_{yy}\frac{\partial h}{\partial y}\right)+\frac{\partial}{\partial z}\left(K_{zz}\frac{\partial h}{\partial z}\right)+W=S_s\frac{\partial h}{\partial t} \quad \text{Eq 1}$$

where $K_{xx}$, $K_{yy}$, and $K_{zz}$ are hydraulic conductivity along the x, y, and z coordinate axes (L/T); $h$ is the hydraulic head (L); $W$ is a volumetric flux per unit volume representing sources and/or sinks, such as recharge and wells (1/T); $S_s$ is the specific storage of the porous material (1/L); and $t$ is time (T). The model is isotropic ($K_{xx} = K_{yy} = K_{zz}$) and heterogeneous, with hydraulic conductivity generally increasing with depth (Figure 1). The groundwater flow system was set to transient. Equation 1 is solved using MODFLOW-2005 (Harbaugh et al., 2005), based on a finite different grid characterized by 241 columns, 201 rows, and 51 layers, with a grid-block size of 5m × 5m × 5m. The flow model is by characterized by a constant head boundary condition on the east and west (see Figure 1), with groundwater recharge applied to the water table (Table 1). Other boundaries are set as "no flow". MODFLOW-2005 calculates the pore velocity field ($\boldsymbol{v} = -\frac{K}{\phi}\cdot\nabla h$, where $\phi$ is the effective porosity), which is then used in the multispecies reactive contaminant transport simulator MT3D-USGS (Bedekar et al., 2016) to solve a system of coupled partial differential equations, each of which represents the mass continuity for the species simulated:

$$\nabla(\phi\cdot\mathbf{D}\cdot\nabla C_i)-\nabla(\phi\cdot\mathbf{v}\cdot C_i)+\mathrm{q}_{s,i}\cdot C_{s,i}+R_i=\frac{\partial(\phi\cdot C_i)}{\partial t} \quad \text{Eq 2}$$

where $C_i$ is the concentration of species $i$ [M/L$^{-3}$], **D** is the hydrodynamic dispersion tensor [L$^2$/T$^1$], $q_{s,i}$ [M/L$^3$] represents the specific discharge for species $i$, $C_{s,i}$[M/L$^3$] represents the concentration of sources for species $i$, and $R_i$ represents the reaction rate of species $i$ [M/L$^3$/T$^1$]. In this case, there are three species ($i = 1,2,3$), and the term $R_i$ depends on ongoing kinetic reactions occurring between 1 electron donor (ED) and 2 electron acceptors (EAs), simulated using a Monod kinetic model developed by Lu et al. (1999), following approaches used in previous studies (Rolle et al., 2008). The stoichiometric reactions between phenol ($C_6H_6O$), which is the ED, and the two EAs, oxygen ($O_2$) and nitrate ($NO_3^-$), are described by the following equations:

(a) $C_6H_6O + 7O_2 \rightarrow 6CO_2 + 3H_2O$ Eq 3

(b) $C_6H_6O + \frac{28}{5}NO_3^- + \frac{28}{5}H^+ \rightarrow 6CO_2 + \frac{14}{5}N_2 + \frac{29}{5}H_2O$ Eq 4

Eq 3 and 4 are presented to illustrate the stoichiometry of the reactions which are considered in Eq 6.

The rate of ED biodegradation ($i = 1$ in Eq. 2) is given by (Lu et al., 1999):

$$r_{ED} = \sum_{j=1}^{2} r_{ED,j} = -\left\{\frac{k_{EA_1} \cdot [EA_1]}{K_{EA_1} + [EA_1]} + \frac{k_{EA_2} \cdot [EA_2]}{K_{EA_2} + [EA_2]} \cdot \frac{K_{I,EA_1}}{K_{EA_1} + [EA_1]}\right\} \cdot [ED] \quad \text{Eq 5}$$

where $[ED]$, $[EA_1]$, and $[EA_2]$ represent the concentration of the ED and the two EAs (M/L$^3$), respectively; $k_{EA_1}$and $k_{EA_2}$ are first-order decay rate constants for the EAs (1/T); $K_{EA_1}$ and $K_{EA_2}$ are the "half saturation" constants for the EAs (M/L$^3$); $K_{I,EA_1}$ (M/L$^3$) is the inhibition constant for the first EA, oxygen, which has the highest Gibbs free energy (Christensen et al., 2000). Correspondingly, the rate of consumption of the two EAs, which affects the concentration of the EAs, ($i = 2,3$ in Eq. 2) is given by:

$$r_{EA_j} = Y_{EA_j} \cdot r_{ED} \quad \text{Eq 6}$$

where $Y_{EA_j}(j = 1,2)$ is the yield coefficient for the EA, that is, the EA mass used per ED unit mass biodegraded, calculated from the stoichiometry in Eqs. 3 and 4 (Table 1).

The mass biodegraded is obtained by integration of the rate of ED biodegradation $r_{ED}$ (Eq 5) over the model domain for the remediation period $T$, that is:

$$M_{bio}(T) = \int_{t=0}^{T} \left[ \int_{\Omega} \theta \cdot r_{ED} \cdot d\Omega \right] dt \quad \text{Eq 7}$$

where Ω represents the 3D model domain, $\theta$ (/) is the effective porosity, $r_{ED}$ (M/L$^3$/T) is the biodegradation rate (Eq 5). This integral is numerically calculated over the model grid and the discretization of the time interval $[0, T]$ adopted in the flow and transport simulation.

### 3.3 Model development and scenarios

The flow and reactive transport models presented in Section 3.2 were used to create a hypothetical phenol plume using data on the physical aquifer characteristics obtained from previous site investigations conducted by third party consultants (Table 1), and research published over the past 25 years (Mayer et al., 2001; Thornton et al., 2001b; Watson et al., 2005). The rationale behind using this approach was not to interpret the actual contamination conditions at the site, but to instead develop a model that is internally coherent and consistent. This enabled a hypothetical but realistic example model to be created, with results that can be extended to other sites with similar characteristic and/or contaminated with coal tar distillate plumes (e.g. Blum et al., 2011).

Figure 1 shows a contaminant plume simulated with this model. This is in excellent agreement with plumes produced in other studies at the site using the same dataset (Mayer et al., 2001; Watson et al., 2005), and is similar to the concentration distribution observed in monitoring surveys conducted at the same time (Williams et al., 2001; Thornton et al., 2001b). To create the numerical model, a regional model with local canals and pumping stations was developed based on data from confidential third-party consultant reports. Recharge was estimated from effective infiltration and applied to the water table. Initial simulations revealed that the most important parameters for the transport model are recharge and hydraulic conductivity. These initial simulations also revealed that the groundwater flow in a 1.2 km$^2$ square area encompassing the plume is steadily east to west, which is supported by site data. Therefore, the original regional flow model was then cropped to a size appropriate for simulating the range of hydraulic gradients observed at the site (horizontal hydraulic gradient of 0.003-0.007). The eastern and western constant head boundary conditions of 103m and 98m, which were acquired from previous groundwater monitoring at the site, were used to simulate the average horizontal hydraulic gradient for the site (0.004). The north and south boundaries are simulated as general head boundaries with linearly decreasing head from east to west, and the bottom boundary is no flow. The contaminant source consists of DNAPL (coal tar) trapped within shallow groundwater at the site, which was simulated as a single 5x5x5 m$^3$ cell (the source term is unknown). In order to generate a plume comparable to that observed at the site, the release of phenols from the

source was simulated at 1344 mg/d over 70 years. This was determined to give the corresponding concentration distribution in the aquifer, with a maximum dissolved concentration of 25,000 mg/l (similar to the source zone) and total plume mass of 34,000 kg. The source was then assumed to be removed (as per conventional remediation practice) before PAT operations commenced (Cohen et al., 1997). As the magnitude of dispersion is a function of the aquifer dispersivity (Ye et al., 2015), values of this coefficient were taken from previous modelling studies at the site (Table 1), which were of the same order as those estimated in other studies (e.g. Cirpka et. al., 1999, 2006; Cupola et al., 2015; Reising, 2018).

Based on the work of Williams et al., (2001) and Thornton et al., (2001 a,b), the nitrate concentration in groundwater at the site varies slightly along the depth, decreasing from 106 mg/l to 91 mg/l between 5-60 mgbl. However, the dissolved oxygen concentration decreases from 9 mg/l to 4.5 mg/l over the same depth interval. These solute profiles were included in the layers for the initial concentration and eastern constant head boundary to develop the spatially variable inputs of EAs in the model. Note that the EA concentrations used correspond to those of the background groundwater (Table 1). In some of the investigated scenarios, groundwater with this EA composition is injected into the aquifer, with the suffix "GW" to denote the results. In other scenarios, groundwater without EAs (with the suffix "GWWEA"), was injected. Monod parameter values from previous studies were used for the kinetic reaction component of the model (Mayer et al., 2001; Watson et al., 2005). Based on unpublished calculations of the reaction rates, the most important parameters that are subject to change in space and time are the ED and EA concentrations. The other Monod parameters are constant. See Figure 1 for more details.

Six numerical modelling scenarios (experiments) were developed for this study (Table 2). Scenario A depicts a longitudinal, vertical cross section of the plume, whereas scenarios B-F depict horizontal cross-sections with wells positioned laterally from the idealised plume centreline and/or on it. The pumping rate ($\bar{Q}$) can be negative (extraction) or positive (injection). The performance of the system in each scenario was compared using ratios of total phenol mass removed ($M_{rem}$) to initial phenol mass ($M_0$), $M_{rem}/M_0$. $M_{rem}$ has two components, $M_{bio}$, the mass of phenol biodegraded, and $M_{ext}$, the mass of phenol extracted. Hence, $M_{rem} = M_{bio} + M_{ext}$. Normalizing $M_{bio}$ and $M_{ext}$ to the initial plume mass, $M_0$, allows the results to be compared directly and shows the relative contribution of mass removal by each process.

For all scenarios except Scenario A the well screen is 5-m long and located approximately 70 mbgl. This pumping depth has the highest aquifer hydraulic conductivity and was selected to allow for higher pumping rates. The wells

in each scenario are pumping for a period $T$ of 10 years. The simulations within each scenario are carried out independently to prevent the effects of previous simulations interfering with subsequent results. For all groundwater (suffix GW) injection sub-scenarios, groundwater with a concentration of 9.28 mg/l of oxygen and 105 mg/l of nitrate (aquifer concentration) was injected. For groundwater without EA (suffix GWWEA) injection scenarios, no EAs are injected. Simulations in each scenario were carried out until the value of $M_{rem}/M_0$ or biodegradation began to decrease. For scenarios where $M_{rem}/M_0$ and biodegradation did not increase, they were capped at 7 simulations, as this was sufficient to evaluate the trend. In all, 68 simulations were conducted.

The following controlling variables were tested in several scenarios, adjusting each for (i) well locations in the longitudinal and transverse horizontal planes, (ii) pumping rates, (iii) effectiveness of an injection vs extraction well, (iv) impact of increasing the pumping rate for 2 wells, (v) impact of increasing the transverse horizontal distance between 2 pumping wells with a constant pumping rate, and (vi) the impact of an injection and extraction well in the same scenario. The aim of these scenarios was to determine strategies which increase $M_{bio}/M_0$ while decreasing or minimizing $M_{ext}/M_0$.

Scenario A investigates the effect of extraction well location along the plume flow path on the enhancement of biodegradation *in situ* (Table 2A). A single extraction well located in the plume interior/centreline is tested in 4 simulations which span the length (L) of the plume. Since the plume flow path is diving to recharge, the plume centreline changes with longitudinal distance and the depths of the well screens change accordingly (between 10 and 70 mbgl) for each simulation to keep the well within the plume interior. The variable in this scenario is L (the x location), which begins at the plume front at 200 m, and is increased by 200 m until near the plume source, at 800 m. The well extracts groundwater at -30 $m^3/d$ for 10 years. It is hypothesized that $M_{bio}/M_0$ and $M_{ext}/M_0$ will increase as longitudinal distance trends to 800 m.

Scenario B investigates the effect of pumping rate on the enhancement of biodegradation *in situ* (Table 2B). The well is consistent for all simulations, located 15m from the plume centreline/interior and at the plume fringe. This scenario has three sub-scenarios: extraction, injection of groundwater without electron acceptors (GWWEA), and injection of groundwater (GW) with the peak concentration of EAs found in the aquifer. The sub-scenarios are labelled as B-Ext, B-GWWEA, and B-GW in Figure 4a. For each sub-scenario, the pumping rate of the well is varied from 5 to 100 $m^3/d$. Seven simulations are run for each sub-scenario. The purpose of having separate groundwater injection scenarios (with and without EAs) is to observe the effect of only plume fringe biodegradation processes, as there is no biodegradation within the plume core when GWWEA is injected. The

297 variable tested is the effect of the pumping rate, the constant well location at the plume fringe and the type of
298 groundwater injected. These are compared with the no-action case, other scenarios, and among the sub-scenarios.
299 The first simulation in Scenario B-Ext is comparable to Scenario A at 800 m, as they have the same pumping rate;
300 the only variable that changes is that the well in Scenario B-Ext is 15 m further away from the plume centreline
301 than in Scenario A at 800 m; thus, the impact of distance can be compared. The difference between pumping at
302 the plume centre vs plume fringe was determined in this comparison. It is hypothesized that $M_{bio}/M_0$ for Scenario
303 B will increase with pumping rate. $M_{ext}/M_0$ will increase with pumping rate only for Scenario B-Ext.

304 Scenario C investigates the effect of lateral well location on the enhancement of biodegradation *in situ* (Table 2C).
305 The scenario has three sub-scenarios: extraction, injection of groundwater without electron acceptors (GWWEA),
306 and injection of groundwater (GW) with the peak concentration of EAs found in the aquifer. The sub-scenarios
307 are labelled as C-Ext, C-GWWEA, and C-GW in Figure 4a. The purpose of having separate groundwater injection
308 scenarios (with and without EAs) is to compare the effect of plume fringe vs core biodegradation processes, as
309 there is no biodegradation within the plume core when GWWEA is injected. Six simulations are run for each sub-
310 scenario. The only changing variable is the north horizontal transverse distance to the plume interior/centreline,
311 which is varied by 20 m each step and then by 10 m for the final two steps. Since Scenario C starts at the plume
312 centreline (d = 0 m), this specific simulation is directly comparable to Scenario A at 800 m; thus, the impact of
313 varying longitudinal vs lateral distance can be directly compared. It is hypothesized that for Scenario C-Ext,
314 $M_{bio}/M_0$ will increase and $M_{ext}/M_0$ will decrease as lateral distance from the plume centreline increases. For
315 Scenario C-GWWEA and C-GW, only $M_{bio}/M_0$ are expected to increase. Therefore, the relevant comparison
316 between Scenario B-Ext and Scenario A at 800 m is the effect of the change in pumping rate.

317 Scenario D investigates the effect of variable pumping rate for two extraction wells on the enhancement of
318 biodegradation *in situ* (Table 2D). The extraction wells are located 15m north and south of the plume centreline
319 (cumulative 30 m lateral distance). The pumping rate is split between the two wells and is varied from 5 to 100
320 $m^3/d$. This scenario is essentially the same as Scenario B-Ext, except with an extra well. The cumulative pumping
321 rate in Scenario D is kept identical to Scenario B-Ext so that the effect of an additional well can be directly
322 compared. It is hypothesized that $M_{bio}/M_0$ and $M_{ext}/M_0$ will increase with the pumping rate.

323 Scenario E investigates the effect of lateral distance between two extraction wells on the enhancement of
324 biodegradation *in situ* (Table 2E). This scenario is identical to Scenario D, except that the lateral distance between
325 the two extraction wells changes during each simulation and the cumulative pumping rate is kept constant. The

distance between the wells starts at 30 m and is increased by 30 m during successive simulations to a maximum of 90 m. A cumulative pumping rate of -60 $m^3$/d was chosen, which is comparable to the mid-range pumping rate in Scenario D and Scenario B. It is hypothesized that $M_{bio}/M_0$ will increase and $M_{ext}/M_0$ will decrease as the distance between the two wells increases.

Scenario F investigates the effect of lateral distance of a doublet injection and extraction well on the enhancement of biodegradation *in situ* (Table 2F). This scenario has two sub-scenarios: extraction combined with injection of groundwater without electron acceptors (GWWEA) and extraction combined with injection of groundwater (GW) with the peak concentration of EAs found in the aquifer. The sub-scenarios are labelled as F-GWWEA and F-GW in Figure 4a. The purpose of having separate groundwater injection scenarios (with and without EAs) is to observe the effect of plume fringe vs plume core biodegradation processes, as there is no biodegradation within the plume core when GWWEA is injected. The lateral distance between the injection and extraction well starts at 15m and is increased by 15m with subsequent simulations, to a maximum of 105m. As with Scenario D, the effect of lateral distance in well spacing is investigated. However, this scenario differs in that one well is an injection well, which may increase plume spreading (and therefore biodegradation) to a greater degree due to the divergent flows caused by injection. The pumping rates are kept constant at 30 and -30 $m^3$/d for the injection and extraction wells, respectively. It is hypothesized that using an injection and extraction well doublet will increase spreading of the plume and enhance $M_{bio}/M_0$ greater than a scenario in which this is done with two extraction wells, and $M_{ext}/M_0$ will decrease as the lateral distance between the two wells increases.

An additional experiment was conducted to consider the effect of dispersivity coefficients on mass removal by biodegradation, as a basis to understand the role of dispersion. The dispersivity in all dimensions was changed for three test cases, with a model duration of 10 years. The dispersivity coefficients were estimated using the regression equation from Xu and Eckstein (1995) and data from Gelhar et al., (1992). Each test case is split into a simulation with "no intervention", in which there are no wells and only intrinsic biodegradation is quantified, and a simulation with groundwater injection at 30 $m^3$/d with a well located 15m lateral to the plume centreline (same location as Scenario B-GW). In case 1, the dispersivity (meters) is the same as the baseline model ($\alpha_x$=1, $\alpha_y$=1e-2, $\alpha_z$=4e-3). In case 2, the dispersivity is reduced 10x from case 1 ($\alpha_x$=0.1, $\alpha_y$=1e-3, $\alpha_z$=4e-4) and in case 3, the dispersivity is increased 10x from case 1 ($\alpha_x$=10, $\alpha_y$=1e-1, $\alpha_z$=4e-2). Beside the dispersivity coefficients, all other parameters are consistent for all cases (Table 1).

## 4 Results and discussion

355 **4.1 Overview of scenario analysis**

356 The outputs from the scenario modelling are shown in Figure 2 as ratios of $M_{bio}/M_0$ and $M_{ext}/M_0$, which are
357 combined under the label $M_{rem}/M_0$, which represents the proportion of total mass removed by pumping and
358 biodegradation (Section 3.3). $M_{bio}/M_0$ is calculated and labelled for each well type, including the extraction and
359 injection well. The prefix "Ext" and "Inj" refer to a scenario which has injection and/or extraction wells,
360 respectively. The suffixes GW (groundwater) and GWWEA (groundwater without EAs) are used to distinguish
361 the injection of water with or without EAs, respectively. The $M_{rem}/M_0$ ratio profiles are reported for $T = 10$ years
362 after the start of the PAT operation, at $t = 0$. The value of $M_{bio}/M_0$ for "no action" is denoted by the "X" on the
363 y-axis in Figure 2, which is a constant value for all panels. This represents 0.69% of the total phenol mass that is
364 biodegraded over 10 years without PAT intervention. As an example, a $M_{ext}/M_0$ ratio of 0.32 implies that the PAT
365 extraction well removed 32% of the phenol mass. A scenario is considered more effective as the value of $M_{bio}/M_0$
366 increases (*i.e.* biodegradation is increased), and more efficient if it also has a lower value of $M_{ext}/M_0$ (*i.e.* less mass
367 to be sent for treatment is removed). Objectives (a) and (b) are addressed in Scenario A-F, whereas objective (c)
368 is addressed in Scenario F.

369 Figure 3 shows the mass biodegraded (kg) in each scenario, which consists of the same data shown Figure 2 before
370 normalization to the initial mass ($M_0$), to allow observing more detail. Figure 4 shows the relative and absolute
371 rankings of all scenarios, with respect to each other and the initial mass. Figure 5 shows the results of the dispersion
372 experiment with 3 dispersion test cases: case 1, where dispersion is the same as the values shown in Table 1; case
373 2, where dispersion is decreased by a factor of 10; and case 3, where dispersion is increased by a factor of 10.
374 Except for Figure 5, the results for each figure are discussed per scenario, from A-F.

375 **4.2 Scenario A**

376 Figure 2A shows that the ratio $M_{bio}/M_0$ remains rather constant, with no significant variation from the no-pumping
377 (no action) case, denoted by the "X" label, which is the same for all graphs. Figure 2A also shows that $M_{ext}/M_0$
378 increases in the simulations as the well location approaches the plume core (800 m). Figure 3A likewise shows
379 that the mass biodegraded remains mostly unchanged, with slightly elevated biodegradation occurring at the
380 plume front ($l$=200 m). Figure 4a shows that Scenario A did not enhance biodegradation above the baseline "no
381 action" and Figure 4b shows that Scenario A only biodegraded 0.69% of the total plume mass. The results of
382 Scenario A indicate that changing the longitudinal well location has no significant effect on biodegradation, at

least for well locations in the plume interior/centreline. The results also indicate that $M_{ext}/M_0$ increases with phenol concentration, as the concentration significantly increases from 200 m to 800 m, which is expected.

As the well is placed at the plume centreline, it is less effective at enhancing biodegradation since the EA ($O_2$ and $NO_3$) concentrations are depleted within the plume very quickly and most biodegradation occurs at the fringe where the plume and EAs mix. At a selected pumping rate (-30 $m^3/d$), the area of influence of the well does not extend beyond the plume fringe, which reduces mixing between the ED and EAs. Extraction in the plume interior/centreline does not enhance mixing or transverse spreading, which has been shown to increase reaction rates in other studies (Rolle et al., 2009; Castro-Alcaca et al., 2012; Sather et al., 2022; 2023). Additionally, groundwater extraction at the plume centre limits biodegradation because the ED is extracted before reacting with the EAs in the background groundwater. These interactions and limitations on biodegradation for this scenario are illustrated in Figure S1-A3, which shows a very weakly developed plume fringe and low biodegradation rate ($r_{ED}$), even compared with the initial plume condition (Figure S1-I3). This well configuration therefore removes phenol mass with no significant biodegradation due to limited dispersive flux of EAs from the background groundwater. Scenario A did not enhance biodegradation above the baseline condition since the radius of influence of the well is not sufficient to induce significant mixing at the plume fringe. This can be seen in Figure S1-A3, where the biodegradation rate is mainly enhanced near the well. While the biodegradation rate in Figure S1-A3 is larger (greater intensity), the overall area where the biodegradation rate is >0 is lower than the initial condition (Figure S1-I3).

### 4.3 Scenario B

Figure 2B shows that the value of $M_{bio}/M_o$ increases with pumping rate for all sub-scenarios, but with a higher contribution to mass removal through biodegradation from the injection sub-scenarios (B-GWWEA and B-GW). Figure 2B also shows that $M_{ext}/M_0$ increases with pumping rate for Scenario B-Ext, as expected. Figure 3B shows the mass removed by biodegradation for each sub-scenario in greater detail. Figure 4a and 4b show that Scenario B-Ext increases $M_{bio}/M_o$ by 50% above "no action" and 0.92% of the plume contaminant mass is biodegraded at the maximum pumping rate. Figure 4a and 4b show that in the GWWEA injection sub-scenario, $M_{bio}/M_o$ is enhanced by 89% above "no action" and 1.32% of the plume mass is biodegraded at the maximum injection rate. Figure 4a and 4b show that in the GW injection sub-scenario, $M_{bio}/M_o$ is enhanced by 128% above "no action" and 1.57% of the plume mass is biodegraded at the maximum injection rate. The GWWEA and GW injection sub-scenarios are 44% and 71% more effective at enhancing biodegradation above no action than the Ext sub-scenario,

respectively. Due to the injection of EAs, the GW case enhanced biodegradation by 19% relative to the GWWEA case (no EAs present). The results of Scenario B indicate that pumping rate has a significant effect on mass removal by biodegradation, and that injection of groundwater is significantly more effective at enhancing biodegradation than groundwater extraction.

The enhancement of biodegradation resulting from an increased pumping rate is attributable to the following. In general, as the pumping rate increases, the plume is spread over a larger area under the spatially varying velocity field created, which results in enhanced dispersive mixing between the ED and EAs (Rolle et al., 2009; Suk et al., 2021; Sather et al., 2022; 2023). For GWWEA injection, biodegradation (represented by $r_{ED}$) is only enhanced in a narrow zone at the plume fringe (Figure S1-B6). For GW injection, biodegradation is enhanced both in the plume interior and at the plume fringe, although the EAs will be rapidly consumed within the plume interior, which may result in their complete depletion (Figure S1-B8 and B9). For GW extraction, biodegradation is enhanced near the well where the ED and EA are mixed, and at the plume fringe (Figure S1-B3 and A3). However, since the extraction well removes mass from the system, it does not enhance the biodegradation rate $r_{ED}$ as much as groundwater injection, where mixing between the ED and EA is more effective and the resultant biodegradation rate is higher (Figure S1-B3 vs B6 and B9).

### 4.3 Scenario C

Figure 2C shows that, except for Scenario C-GW, the value of $M_{bio}/M_0$ increases with lateral distance from the plume centreline/interior up to 60 m, and then appears to stay constant for the remainder of the experiment. Scenario C-GWWEA and C-GW start at a higher value of $M_{bio}/M_0$ than Scenario C-Ext, but eventually converge to approximately the same value at 60 m. Figure 3C shows more detail, in that after 60 m biodegradation for C-Ext and C-GWWEA begins to slightly decrease. Scenario C-GW responds differently to the change in lateral distance than the other sub-scenarios. Figure 3C shows that C-GW is most effective in the plume interior/centreline (0 m), and begins to decline, eventually converging to the same value of biodegradation as the other sub-scenarios. Figure 4a and 4b show that for Scenario C-Ext and GWWEA, $M_{bio}/M_o$ is enhanced by ~62% above "no action" and ~1.13% of the total phenol mass is biodegraded. Figure 4a and 4b also show that for C-GW, $M_{bio}/M_o$ is enhanced by ~68% above "no action" and 1.16% of total phenol mass is biodegraded. Figure 2C and 3C show that, initially, at a distance of 0 m (plume centreline), GW injection is 23% more effective in enhancing biodegradation than GWWEA injection, 73% more effective than C-Ext. In addition, Scenario C-GW is 73% more effective than Scenario A at 800m (Figure 2A and 3A).

The reason why $M_{bio}/M_0$ is not enhanced beyond a lateral distance of 60 m is due to the capture zone of the well having a reduced influence on the plume. This is supported by the significant decrease in $M_{ext}/M_o$ that occurs after 40 m, trending to zero after 60 m (Figure 2C). Since no ED (phenol) mass is removed, the well increases the value of $M_{bio}/M_o$ (i.e. stimulates biodegradation) by increasing plume spreading and the plume fringe interface as the plume is pulled further away from the center (Sather et al., 2022; 2023).

The initial and final values of phenol concentration, dissolved $O_2$ concentration and biodegradation rate $r_{ED}$ for the Scenario C-Ext simulation are compared with the initial plume condition in Figure S1, illustrating the dynamic nature of the plume fringe interface and biodegradation under pumping. These simulations and those more generally in Figure S1 show stretching and folding of the plume due to active spreading induced by the arrangement of the PAT system in each scenario, also documented by Piscopo et al. (2013) in a similar study. As the extraction well located lateral to the plume centreline removes contaminant mass, the phenol concentration is decreased and the plume fringe surface area is increased by lateral spreading (SI I1 vs SI C1) of the plume during pumping, allowing greater mixing of dissolved EAs (note the increased $O_2$ footprint) across the interface (SI I2 vs SI C2). Ultimately, this increases the spatial extent of the interface and rate of biodegradation $r_{ED}$ at the plume fringe compared with the initial condition (SI I3 vs SI C3). By changing the plume flow direction in this way, the reaction front (plume fringe) is aligned perpendicular to the local flow field towards the extraction well. In this case mixing is dominated by longitudinal dispersion in the direction of flow, which is much greater than transverse dispersion, resulting in enhanced biodegradation (Sather et al., 2022; 2023).

With each sub-scenario at their peak performance, GW injection at 0 m is marginally the most effective strategy overall as it significantly enhances biodegradation while reducing mass extraction For example, it is ~2.6% more effective than GWWEA injection or C-Ext at 60 m. Groundwater injection is effective for this enhancement because biodegradation inside the plume is limited by the depletion of available EAs (oxygen and nitrate) and the flux of these EAs into the plume, as induced by the PAT system. These points highlight that while the injection of groundwater at the plume centre can significantly enhance biodegradation compared to injection of EA-depleted groundwater or groundwater extraction at the same location, increasing plume spreading by pumping laterally to the plume is equally important.

### 4.4 Scenario D

Figure 2D shows that $M_{bio}/M_0$ remains mostly constant as the pumping rate is increased for both extraction wells. This is confirmed by Figure 3D (enhanced resolution) which shows the absolute contaminant mass biodegraded.

The lowest pumping rate of -5 $m^3/d$ resulted in the highest value of $M_{bio}/M_0$. Figure 4a and 4b show that Scenario D enhanced mass removal by biodegradation by 8% over the no action case and removed 0.75% of the plume mass (vs 0.69% for "no action"). These results indicate that increasing the pumping rate for two extraction wells located at a constant lateral distance (30 m) has little to no effect on biodegradation.

The results also indicate that extracting groundwater symmetrically from two wells is less effective compared to a single well with similar pumping rate, such as Scenario B-Ext. This is attributed to a decrease in dispersive mixing of EAs within the plume caused by the proximity of the two wells, which have an overlapping radius of influence. This is evidenced by the absence of biodegradation at or near the wells (Figure S1, D3). In Scenario D both the maximum value of the biodegradation rate and area in which biodegradation occurs is reduced (Figure S1, I3 vs D3). In Scenario B, the well promotes dispersive mixing of the background groundwater and plume, increasing the value of $M_{bio}/M_o$ within the well capture region (Figure S1, B3). However, in this dual well configuration (Scenario D), the background groundwater is drawn into the plume margin at each side. At high pumping rates, adequate mixing between the ED and EA does not occur because the phenol mass is excessively removed by the combined action of the two extraction wells, which are located too close together (Figure S1, D1-D3). Also, at low pumping rates, these extraction wells cannot appropriately influence the region between them to the same degree, as the EAs are instead drawn away from the plume toward the extraction well on either side. The performance of this scenario could be improved if the lateral distance between the two wells was greater.

Despite Scenario B having only one well, more contaminant mass was extracted than in Scenario D. This is because the two wells in Scenario D are located 30 m apart, and the pumping rate is split between them (up to -50 $m^3/d$ each), rather than concentrated (-100 $m^3/d$) in a single cell. The strategy in Scenario D is therefore not effective because biodegradation is limited by the very close spacing of the wells and the contaminant mass extracted is large, implying increased operational costs for subsequent groundwater treatment.

### 4.5 Scenario E

Figure 2E shows that $M_{bio}/M_0$ increases with lateral distance between the two extraction wells. At the first point in Scenario E, $M_{bio}/M_0$ and "no action" are equal, indicating that at a lateral distance of d=30 m, biodegradation was not enhanced above baseline conditions. Figure 2E also shows that the most effective arrangement is for each well to be placed 45m away from the plume centreline (i.e. the distance between them is 90 m). Figure 4a and 4b show that at this optimal position, 0.9% of the total plume mass was biodegraded compared to the no action case (0.7%), with a maximum enhancement in $M_{bio}/M_o$ of ~24% above "no action". The enhancement in

biodegradation is due to the same processes as in Scenario C-Ext and C-GWWEA. As the lateral distance between the extraction wells increases, phenol biodegradation is enhanced by the greater degree of dispersive mixing created by this interaction.

Beyond the 45m distance, the overlap between the capture zone of the two wells and the plume decreases. This is supported by the decrease in $M_{ext}/M_o$, which indicates that the plume is unaffected by this well arrangement. The value of $M_{ext}/M_o$ decreases after a well separation of 60 m because contaminant concentrations decrease quickly at the plume margin (Thornton et al, 2001a). The extent of biodegradation at the plume fringe is also limited by the supply of organic contaminants to this interface, controlled by the dispersive mixing. Unlike Scenario D, Scenario E enhances plume spreading and mixing because the pumping rates are lower and the wells are further apart, such that the ED and EAs are not removed as rapidly and adequate mixing between the plume and groundwater is possible to support biodegradation. Further analysis shows that this scenario results in significant spreading of the plume and enlargement of the plume fringe between the extraction wells, as shown by the increased footprint of the dissolved $O_2$ concentration gradient across this interface (Figure S1-E2) and corresponding zone of enhanced biodegradation rate, $r_{ED}$ (Figure S1-E3).

### 4.6 Scenario F

Figure 2F shows that the value of $M_{bio}/M_o$ increases with the lateral distance between the extraction and injection wells. For both the GWWEA and GW sub-scenarios, $M_{bio}/M_0$ reached its highest value at a lateral distance of 90 m, after which it begins to decline.

Figure 4a and 4b show that 1.2% and 1.4% of the total phenol mass were biodegraded for each sub-scenario, respectively. This is respectively an enhancement of 67% and 100% above "no action" in mass removal by biodegradation (Figure 4a). For this arrangement GW injection was ~18% more effective at enhancing biodegradation than GWWEA injection, as shown by the increased mass biodegraded (Figure 4a). This difference arises because biodegradation occurs within the plume interior (where the injection well is located) and at the plume fringe (where the extraction well is located) in the GW injection sub-scenario. However, biodegradation only occurs at the plume fringe in the GWWEA sub-scenario, as the latter has no EA suite to support biodegradation directly, and the injected GWWEA simply enhances dispersive mixing without supplementing the EA supply.

After a well separation distance of 90 m, $M_{ext}/M_o$ decreases sharply to zero, as progressively less contaminant mass is extracted, and $M_{bio}/M_o$ begins to decrease, indicating a reduced influence of the well on biodegradation in the plume (Figure 2F). Overall, this scenario was respectively 87% and 62% more effective at enhancing biodegradation than using two concurrent extraction wells, as in Scenario D and E. However, the plume fringe was enhanced much less by the well and pumping arrangement in Scenario F, as opposed to Scenario D (compare Figure S1-F3 and Figure S1-F6 to Figure S1-E3). Nonetheless, the biodegradation rate in Scenario F-GW is generally higher than in Scenario F-GWWEA and Scenario D, which results in higher overall mass removal through biodegradation.

The performance of the combined PAT-NA system in the different scenarios is compared in Figure 4 relative to the "no action" case. This shows that groundwater injection in Scenario B-GW was most effective in removing contaminant mass (Figure 4a) and enhancing biodegradation (Figure 4b) relative to the other scenarios. Over 500 kg of contaminant mass was biodegraded using groundwater injection within Scenario B (Figure 4b). The arrangement of pumping wells in this scenario, with a fixed location at the plume fringe and continuous supply of $O_2$ and $NO_3$ in the injected groundwater, ensures dispersive mixing at the plume fringe is enhanced and biodegradation is not EA limited. While the mass biodegraded in these scenarios is a modest percentage (ca. 2%) of the overall plume, this simply reflects the significant mass of dissolved contaminant in groundwater at the site; the concentration of phenol is several orders of magnitude higher than the concentration of the EAs. Moreover, the mass biodegraded also reflects the low value of aquifer transverse dispersivity at this site, which limits dispersive mixing in the plume.

### 4.7 Effect of dispersion on biodegradation

Figure 5 shows a hypothetical experiment which illustrates the effect of dispersion on biodegradation, as assessed by comparing numerical simulations of the contaminant mass biodegraded for different values of the dispersivity coefficients. A 10-fold increase of the dispersivity coefficients (case 3) above the baseline model (case 1) enhances the biodegradation by approximately 360%, whereas a 10-fold decrease (case 2) reduces biodegradation by only 12%, indicating that the original dispersivity value (case 1) is already quite low for a solute plume of that scale (Gelhar et al., 1992; Xu and Eckstein, 1995). GW injection enhances biodegradation by approximately 96% for case 1 and 2, and by 22% for case 3 (Figure 5). Higher values of dispersivity coefficients result in greater plume spreading in all dimensions, which increases the dispersive mixing between the ED and EAs, as well as the EA flux into the plume to stimulate biodegradation. This feature is evident in several scenarios (e.g. C and E) from

555 the increased size of the plume fringe interface under pumping, and the corresponding greater spatial development
556 of zones with an increased biodegradation rate (Figure S1). GW injection further enhances biodegradation for the
557 same reason, but with diminishing returns at higher values of the dispersivity coefficients. This is likely due to
558 the plume becoming very dilute in case 3, which reduces the biodegradation rate $r_{ED}$ ; the injection well should
559 be located in a more concentrated region of the plume in order to be more effective.

560 **5. Conclusion**

561 This research examined the design of conventional pump and treatment (PAT) systems to increase the *in situ*
562 biodegradation of organic contaminants in groundwater, by addressing potential limitations (electron acceptor
563 supply) on the relevant processes. The aim was to identify the effect of system variables on plume remediation to
564 increase contaminant mass removal by enhancement of biodegradation, as a proof-of-concept evaluation and basis
565 to optimise the system design for best performance. Six scenarios were developed to evaluate the design of the
566 PAT system with these variables, using a 3-D numerical model (MODFLOW and MT3D-USGS) constructed with
567 historical site characterisation data from a chemical manufacturing plant on a UK sandstone aquifer. Using this
568 data, a "synthetic plume" was created in the model to investigate the scenarios in this conceptual analysis. The
569 contaminants in groundwater at the site were all converted into equivalent concentrations of phenol (the
570 predominant contaminant) for the modelling. A Monod formulation was used in the model to simulate the kinetic
571 reactions between phenol and different electron acceptors (dissolved oxygen and nitrate) involved in
572 biodegradation. A 10-year scenario with no active wells and passive natural attenuation was used as a control to
573 compare the additional contribution of biodegradation to mass removal in the groundwater.

574 The scenario modelling showed that the enhancement of biodegradation depends on the location, number,
575 pumping rate and distance between well location(s) in the PAT scheme. Placing the PAT wells too close together
576 limits biodegradation rates and extraction in the plume interior/centreline is less effective than injection in the
577 same location. Since the extraction well removes contaminant mass from the system, this reduces the overall
578 biodegradation rate $r_{ED}$ in space and time, as this is strongly influenced by phenol concentration. In general,
579 injection enhances plume fringe reactions by increasing dispersive mixing through the creation of divergent flows.
580 As the wells are moved laterally outward from the plume centreline, the mass extracted decreases and mass
581 biodegraded increases. The most effective scenarios are injection of groundwater with electron acceptors at 15m
582 from the plume interior/centreline (scenario B-GW), and injection of groundwater with electron acceptors in the
583 plume centreline combined with an extraction well that is located away from the plume centreline (Scenario F-

584 GW). The PAT system enhances *in situ* biodegradation of contaminants by (i) increasing dispersive mixing
585 between solutes in the plume and background groundwater, and (ii) increasing the flux of dissolved electron
586 acceptors into the plume from the background groundwater in zones (e.g. plume fringe) which have high
587 biodegradation potential. Enhanced mixing also increases contaminant dilution and can remove factors which are
588 inhibitory to biodegradation. The analysis shows that biodegradation was significantly improved with PAT
589 intervention above the "no action" case, with an increase of 100-128% in mass biodegraded. The pumping rate is
590 the most effective (and controllable) intervention to enhance biodegradation, as it increases the EA flux into the
591 plume. Furthermore, groundwater extraction at the plume fringe is the most efficient basis to increase the surface
592 area of this interface and enhance solute mass transfer across it by dispersion.

593 Future studies should identify how to minimize the diminishing returns observed with multi-well configurations.
594 If the effectiveness of a single well could be multiplied or scaled (Scenario C-Ext), this could potentially shorten
595 remediation timeframes significantly. The effectiveness of different combinations of EAs in the injected
596 groundwater for biodegradation should also be considered, although this will likely depend on the contaminant
597 mixture in specific cases. Overall, the approach illustrated here offers new opportunities to integrate PAT with
598 natural attenuation as a management strategy at sites where groundwater is contaminated by organic chemicals.

599 **6. References**

600 Amos, R., Bekins, B. A., Delin, G. N., Cozzarelli, I. M., Blowes, D. W. and Kirshtein, J. D. (2011). Methane
601 oxidation in a crude oil contaminated aquifer: Delineation of aerobic reactions at the plume fringes. Journal of
602 Contaminant Hydrology, 125, 13-25.

603 Anneser, B., Einsiedl, F., Meckenstock, R. U., Richters, L., Wisotzky, F. and Griebler, C. (2008). High-resolution
604 monitoring of biogeochemical gradients in a tar oil-contaminated aquifer. Applied Geochememistry, 23,
605 1715−1730.

606 Anneser, B., Pilloni, G., Bayer, A., Lueders, T., Griebler, C., Einsiedl, F. and Richters, L. (2010). High resolution
607 analysis of contaminated aquifer sediments and groundwater—What can be learned in terms of natural
608 attenuation? Geomicrobiology Journal, 27, 130-142, DOI: 10.1080/01490450903456723.

609 Antelmi, M., Francesca Renoldi, F. and Alberti, L. (2020). Analytical and numerical methods for a preliminary
610 assessment of the remediation time of pump and treat systems. Water 2020, 12(10), 2850;
611 https://doi.org/10.3390/w12102850.

612 Bagtzoglou, A. C., and Oates. P. M. (2007). Chaotic advection and enhanced groundwater remediation. Journal
613 of Materials in Civil Engineering, 19, 75-83.

614 Baker, K. Bottrell, S. H., Thornton, S. F., Peel, K. and Spence, M. J. (2012). Effect of contaminant concentration
615 on in-situ bacterial sulphate reduction and methanogenesis in a phenol-contaminated aquifer. Applied
616 Geochemistry, 27, 2010-2018.

617 Bauer, R. D., Rolle, M., Bauer, S., Eberhardt, C., Grathwohl, P., Kolditz, O., Meckenstock, R. U. and Griebler,
618 C. (2009). Enhanced biodegradation by hydraulic heterogeneities in petroleum hydrocarbon plumes. Journal of
619 Contaminant Hydrology, 105, 56-68.

620 Bayer, P., Finkel, M. and Teutsch, G. (2004). Combining pump-and-treat and physical barriers for contaminant
621 plume control. Ground Water, 42, 42, 856-867.

622 Bedekar, V., Morway, E. D., Langevin, C. D. and Tonkin, M. J. (2016). MT3D-USGS version 1: A US Geological
623 Survey release of MT3DMS updated with new and expanded transport capabilities for use with MODFLOW.
624 Techniques and Methods 6-A53.

625 Blum, P., Sagner, A., Tiehm, A., Martus, P., Wendel, T. and Grathwohl, P. (2011). Importance of heterocylic
626 aromatic compounds in monitored natural attenuation for coal tar contaminated aquifers: A review. Journal of
627 Contaminant Hydrology, 126, 181-194.

628 Brad, T., Obergfell, C., van Breukelen, B. M., van Straalen, N. M. and Roling, W. F. M. (2013). Spatiotemporal
629 variations in microbial communities in a landfill leachate plume. Ground Water Monitoring and Remediation, 33,
630 4, 69-78. 10.1111/gwmr.12022.

631 Chapelle, F. H. (2000). Ground-water microbiology and geochemistry, 2nd edition. John Wiley & Sons, pp. 496.

632 Christensen, T. H., Bjerg, P. L., Banwart, S. A., Jakobsen, R., Heron, G. and Albrechtsen, H-J. (2000).
633 Characterization of redox conditions in groundwater contaminant plumes: Journal of Contaminant Hydrology
634 Journal of Contaminant Hydrology, 45, 165-241.

635 Chu, M., Kitanidis, P. K. and McCarty, P. L. (2005). Modeling microbial reactions at the plume fringe subject to
636 transverse mixing in porous media: When can the rates of microbial reaction be assumed to be instantaneous?
637 Water Resources Research, 41, W06002, doi:10.1029/2004WR003495.

638 Cohen, R. M., Mercer, J. W., Greenwald, R. M. and Beljin, M. S. (1997). Design guidelines for conventional
639 pump-and-treat systems. Ground Water Issue. EPA/540/S-97/504

640 Cirpka, O. A., Frind, E. O. and Helmig, R. (1999). Numerical simulation of biodegradation controlled by
641 transverse mixing. Journal of Contaminant Hydrology, 40, 159−182.

642 Cirpka, O. A., Olsson, A., Ju, Q., Rahman, A. R. and Grathwohl, P. (2006). Determination of transverse dispersion
643 coefficients from reactive plume length. Ground Water, 44, 212–221.

644 CRC CARE (2019). Technology Guide: Groundwater – pump and treat, National Remediation Framework, CRC
645 for Contamination Assessment and Remediation of the Environment, Newcastle, Australia. pp.39.

646 Cribbin, L. B., Winstanley, H. F. Mitchell, S. L., Fowler, A. C. and Sander, G. C. (2014). Reaction front formation
647 in contaminant plumes. Journal of Contaminant Hydrology, 171, 12–21.

648 Cupola, F., Tandaa, M. G. and Zaninia, A. (2015). Laboratory estimation of dispersivity coefficients. Procedia
649 Environmental Sciences, 25, 74-81.

650 Day, M. J., and Gulliver, T. (2003). Natural attenuation of tert-butyl alcohol at a Texas chemical plant. In MTBE
651 remediation handbook (E. E. Moyer, and P. T. Kostecki, Eds.), pp. 541-560. Amherst, MA: Amherst Scientific
652 Publishers.

653 Dakins, M. E., Porter, P. S., West, M. and Rao, S. T. (1996). Using uncensored trace-level measurements to detect
654 trends in ground water contamination. Water Resources Bulletin, 32, 799-805.

655 Eckert, D., Massimo, R. and Cirpka, O. A. (2012). Numerical simulation of isotope fractionation in steady-state
656 bioreactive transport controlled by transverse mixing. Journal of Contaminant Hydrology, 140, 95-106.
657 10.1016/j.jconhyd.2012.08.010

658 Eckert, D., Kürzinger, P., Bauer, R., Griebler, C. and Cirpka, O. A. (2015). Fringe-controlled biodegradation
659 under dynamic conditions: Quasi 2-D flow-through experiments and reactive-transport modeling. Journal of
660 Contaminant Hydrology, 172, 100-111.

661 Einsiedl, F., Pilloni, G., Ruth-Anneser, B., Lueders, T. and Griebler, C. (2015). Spatial distributions of sulphur
662 species and sulphate-reducing bacteria provide insights into sulphur redox cycling and biodegradation hot-spots
663 in a hydrocarbon-contaminated aquifer. Geochmica et Cosmochimca Acta, 156, 207-221.
664 10.1016/j.gca.2015.01.014.

665 Elliott, D. R., Scholes, J. D., Thornton, S. F., Rizoulis, A., Banwart, S. A. and Rolfe, S. A. (2010). Dynamic
666 changes in microbial community structure and function in phenol-degrading microcosms from a contaminated
667 aquifer. FEMS Microbial Ecology, 71, 247-259.

668 Fahrenfeld, N., Cozzarelli, I., Bailey, Z. and Pruden, A. (2014). Insights into biodegradation through depth-
669 resolved microbial community functional and structural profiling of a crude-oil contaminant plume. Microbial
670 Ecology, 68, 453−462.

671 Gelhar, L.W., Welty, C. and Rehfeldt, K.R. (1992). A critical review of data on field-scale dispersion in aquifers.
672 Water Resources Research, 28, 1955-1974.

673 Gutierrez-Neri, M., Ham, P. A. S., Schotting,R. J. and Lerner, D. N. (2009). Analytical modelling of fringe and
674 core biodegradation in groundwater plumes. Journal of Contaminant Hydrology, 107, 1-1-9.doi:
675 10.1016/j.jconhyd.2009.02.007.

676 Guo, Z., Brusseau, M. L. and Fogg, G. E. (2019). Determining the long-term operational performance of pump
677 and treat and the possibility of closure for a large TCE plume. Journal of Hazardous Materials, 365, 796–803. doi:
678 10.1016/j.jhazmat.2018.11.057.

679 Harbaugh, A.W. (2005). MODFLOW-2005, the US Geological Survey modular ground-water model: the ground-
680 water flow process.

681 Jobelius, C. Ruth, B. Griebler, C. Meckenstock, R. U., Hollender, J., Reineke, A., Frimmel, F. H. and Zwiener,
682 C. (2011). Metabolites indicate hot spots of biodegradation and biogeochemical gradients in a high-resolution
683 monitoring well. Environmental Science and Technology, 45, 474−481.

684 Jones, I., Lerner, D. N. and Thornton, S. F. (2002). A modelling feasibility study of hydraulic manipulation: A
685 groundwater restoration concept for reluctant contaminant plumes. In *GQ2001: Natural and Enhanced*
686 *Restoration of Groundwater Pollution*, Sheffield, U.K., 16-21 June 2001. (eds, Thornton, S.F & Oswald, S.O.),
687 IAHS Publ. No. 275, 525-532.

688 Larentis, M., Hoermann, K. and Lueders, T. (2013). Fine-scale degrader community profiling over an
689 aerobic/anaerobic redox gradient in a toluene-contaminated aquifer. Environmental Microbiology Reports, 5, 225-
690 234. 10.1111/1758-2229.12004

691 Lerner, D. N., Thornton, S. F., Spence, M. J., Banwart, S. A., Bottrell, S. H., Higgo, J. J., Mallinson, H. E. H.,
692 Pickup, R. W. and Williams, G. M. (2000). Ineffective natural attenuation of degradable organic compounds in a
693 phenol-contaminated aquifer. Ground Water, 38, 922-928.

694 Lorah, M. M., Cozzarelli, I. M. and Boehlke, J. K. (2009). Biogeochemistry at a wetland sediment-alluvial aquifer
695 interface in a landfill leachate plume. Journal of Contaminant Hydrology, 105, 99-117.
696 10.1016/j.jconhyd.2008.11.008.

697 Mackay, D. M. and Cherry, J. A. (1989). Groundwater contamination: pump-and-treat remediation.
698 Environmental Science and Technology, 23, 630–636. https://doi.org/10.1021/es00064a001

699 Maier, U., Ruegner, H. and Grathwohl, P. (2007). Gradients controlling natural attenuation of ammonium.
700 Applied Geochemistry, 22, 12, 2606-2617. 10.1016/j.apgeochem.2007.06.009.

701 Mayer, K. U., Benner, S. G., Frind, E. O. Thornton, S. F. and D. N. Lerner. D. N. (2001). Reactive transport
702 modeling of processes controlling the distribution and natural attenuation of phenolic compounds in a deep
703 sandstone aquifer. Journal of Contaminant Hydrology, 53, 341-368.

704 McLeod, H.C., Roy, J.W., Slater, G.F. and Smith, J.E. (2018). Anaerobic biodegradation of dissolved ethanol in
705 a pilot-scale sand aquifer: Variability in plume (redox) biogeochemistry. Journal of Contaminant Hydrology, 208,
706 35-45. 10.1016/j.jconhyd.2017.12.002.

707 McDade, J. M., Kulkarni, P.R., Seyedabbasi, M. A., Newell, C. J., Gandhi, D., Gallinatti, J. D., Cocianni, V. and
708 Ferguson, D. J. (2013). Matrix diffusion modeling applied to long-term pump-and-treat Data: 1. Method
709 development. Remediation Journal, 23, 71-91.

710 Meckenstock, R. U., Elsner, M., Griebler, G., Lueders, T., Stumpp, C., Aamand, J., Agathos, S. N., Albrechtsen,
711 H-J., Bastiaens, L., Bjerg, P. L., Boon, N., Dejonghe, W., Huang, W. E., Schmidt, S. I., Smolders, E., Sørensen,
712 S. R., Springael, D. and van Breukelen, B. (2015). Biodegradation: Updating the concepts of control for microbial
713 cleanup in contaminated aquifers. Environmental Science and Technology, 49, 7073−7081.
714 http://dx.doi.org/10.1021/acs.est.5b00715.

715 Mujica-Alarcon, J. F., Thornton, S. F. and Rolfe, S. A. (2021). Long-term dynamic changes in attached and
716 planktonic microbial communities in a contaminated aquifer. Environmental Pollution, 277, 116765,
717 https://doi.org/10.1016/j.envpol.2021.116765

National Research Council (2013). Alternatives for managing the nation's complex contaminated groundwater sites. The National Academies Press, pp.408.

Neupauer, R. M., Sather, L. J., Mays, D. C., Crimaldi, J. P. and Roth, E. J. (2020). Contributions of pore-scale mixing and mechanical dispersion to reaction during active spreading by radial groundwater flow. Water Resources Research, 56, e2019WR026276. doi.org/10.1029/2019WR026276.

Olaniran, A. O., Pillay, D. and Pillay, B. (2008). Aerobic biodegradation of dichloroethenes by indigenous bacteria isolated from contaminated sites in Africa. Chemosphere, 73, 24-29. 10.1016/j.chemosphere.2008.06.003.

Pickup, R. W., Rhodes, G., Alamillo, M. L., Mallinson, H. E. H., Thornton, S. F. and Lerner, D. N. (2001). Microbiological analysis of multilevel borehole samples from a contaminated groundwater system Journal of Contaminant Hydrology, 53, 269-284.

Pilloni, G., Bayer, A., Ruth-Anneser, B., Fillinger, L., Engel, M., Griebler, C. and Tillmann Lueders, T. (2019). Dynamics of hydrology and anaerobic hydrocarbon degrader communities in a tar-oil contaminated aquifer. Microorganisms, 7, 46, doi:10.3390/microorganisms7020046.

Piscopo, A. N., Neupauer, R. M. and Mays, D. C. (2013). Engineered injection and extraction to enhance reaction for improved in situ remediation. Water Resources Research, 49, 3618-3625.

Prommer, H., Tuxen, N. and Bjerg, P. L. (2006). Fringe-controlled natural Attenuation of phenoxy acids in a landfill plume: Integration of field-scale processes by reactive transport modelling. Environ. Sci. Technol., 40, 15, 4732–4738.

Prommer, H., Anneser, B., Rolle, M., Einsiedl, F. and Griebler, C. (2009). Biogeochemical and isotopic gradients in a BTEX/PAH contaminant plume: Model-based interpretation of a high-resolution field data set. Environmental Science and Technology, 43, 21, 8206–8212https://doi.org/10.1021/es901142a.

Reising, L. J. (2018). Effects of active and passive spreading on mixing and reaction during groundwater remediation by engineered injection and extraction. PhD thesis. University of Colorado, pp. 119.

Rizoulis, A., Elliott, D. R., Rolfe, S. A., Thornton, S. F., Banwart, S. A., Pickup, R. W. and Scholes, J. S. (2013). Diversity of planktonic and attached bacterial communities in a phenol-contaminated sandstone aquifer. Microbial Ecology, 66, 84-95.

744 Rolle, M., Clement, T. P., Sethi, R. and Di Molfetta, A. (2008). A kinetic approach for simulating redox-controlled
745 fringe and core biodegradation processes in groundwater: model development and application to a landfill site in
746 Piedmont, Italy. Hydrological Processes, 22, 4905-4921. 10.1002/hyp.7113.

747 Salowsky, H., Schafer, W., Schneider, A.-L., Muller, A., Dreher, C. and Tiehm, A. (2021). Beneficial effects of
748 dynamic groundwater flow and redox conditions on natural attenuation of mono-, poly-, and NSO-heterocyclic
749 hydrocarbons. Journal of Contaminant Hydrology, 243, 103883. 10.1016/j.jconhyd.2021.103883.

750 Sather, L. J., Neupauer, R. M., Mays, D. C., Crimaldi, J. P. and Roth, E. J. (2022). Active spreading: Hydraulics
751 for enhancing groundwater remediation. Journal of Hydrologic Engineering, 27, p.04022007.

752 Sather, L. J., Roth, E. J., Neupauer, R. M., Crimaldi, J. P. and Mays, D. C. (2023). Experiments and simulations
753 on plume spreading by engineered injection and extraction in refractive index matched porous media. Water
754 Resources Research, 59, p.e2022WR032943.

755 Schmieman, E. A., Petersen, J. N., Yonge, D. R., Johnstone, D. L., Bereded S. Y., Apel, W. A., and Turick, C. E.
756 (1997). Bacterial reduction of chromium. Applied Biochemistry and Biotechnology. 63-5, 855-864.
757 10.1007/BF02920481.

758 Speight, J. G. (2020). Natural water remediation. Butterworth-Heinemann, Elsevier, pp.394.

759 Spence, M. J., Bottrell, S., Thornton, S. F. and Lerner, D. N. (2001) Isotopic modelling of the significance of
760 sulphate reduction for phenol attenuation in a polluted aquifer Journal of Contaminant Hydrology, 53, 285-304.

761 Spence, M. J., Bottrell, S. H., Thornton, S. F., Richnow, H. and Spence, K. H. (2005). Hydrochemical and isotopic
762 effects associated with fuel biodegradation pathways in a chalk aquifer. J. of Contaminant Hydrology, 79, 67-88.

763 Suk, H. Chen, J-S., Park, E. Han, W. S. and Kihm, Y. H. (2021). Numerical evaluation of the performance of
764 injection/extraction well pair operation strategies with temporally variable injection/pumping rates. Journal of
765 Hydrology, 598, 126494. https://doi.org/10.1016/j.jhydrol.2021.126494

766 Suthersan, S., Killenbeck, E., Potter, S., Divine, C. and LeFrancois, M. (2015). Resurgence of pump and treat
767 solutions: Directed groundwater recirculation. Groundwater Monitoring and Remediation, 35, 2, 23-29.

768 Thornton, S. F., Quigley, S., Spence, M. J., Banwart, S. A., Bottrell, S. and Lerner, D. N. (2001a). Processes
769 controlling the distribution and natural attenuation of dissolved phenolic compounds in a deep sandstone aquifer.
770 Journal of Contaminant Hydrology, 53, 233-267.

771 Thornton, S. F., Lerner, D. N., and Banwart. S. A. (2001b). Assessing the natural attenuation of organic
772 contaminants in aquifers using plume-scale electron and carbon balances: model development with analysis of
773 uncertainty and parameter sensitivity. Journal of Contaminant Hydrology, 53, 199-232.

774 Thornton, S. F., Bottrell, S. H., Spence, K. S., Pickup, R., Spence, M. J., Shah, N., Mallinson, H. E. H. M. and
775 Richnow, H. H. (2011). Assessment of MTBE biodegradation in contaminated groundwater using $^{13}C$ and $^{14}C$
776 analysis: Field and laboratory microcosm studies. Applied Geochemistry, 26, 828-837.

777 Thornton, S. F., Baker, K. M., Bottrell, S. H., Rolfe, S. A., McNamee, P., Forrest, F., Duffield, P., Wilson, R. D.,
778 Fairburn, A. W. and Cieslak, L. A. (2014). Enhancement of *in situ* biodegradation of organic compounds in
779 groundwater by targeted pump and treat intervention. Applied geochemistry, 48, 28-40.

780 Thornton, S. F. (2019). Natural attenuation of hydrocarbons in groundwater. In : Consequences of Microbial
781 Interactions with Hydrocarbons, Oils, and Lipids: Biodegradation and Bioremediation, Handbook of Hydrocarbon
782 and Lipid Microbiology. Steffan, R. (ed.), Springer International Publishing, DOI 10.1007/978-3-319-44535-9_3-
783 1, pp.171-195.

784 Topinkova, B., Nesetril, K., Datel, J., Nol, O. and Hosl P. (2007). Geochemical heterogeneity and isotope
785 geochemistry of natural attenuation processes in a gasoline-contaminated aquifer at the Hnevice site, Czech
786 Republic. Hydrogeology Journal, 15, 961-976. 10.1007/s10040-007-0179-8.

787 Truex, M., Johnson, C., Macbeth, T., Becker, D., Lynch, K., Giaudrone, D., Frantz, A. and Lee, H. (2017).
788 Performance assessment of pump-and-treat systems. Groundwater Monitoring and Remediation, 37, 3, 28-44.

789 Tuxen, N., Albrechtsen, H.-J., Bjerg, P. L. (2006). Identification of a reactive fringe zone at a landfill leachate
790 plume fringe using high-resolution sampling and incubation techniques. J. Contam. Hydrol. 85, 179–194.

791 USDoD (1998). Evaluation of DoD waste site groundwater pump-and-treat operations. Report No. 98-090. U.S.
792 Department of Defense. pp. 68.

793 USEPA (1990). Basics of pump-and-treat ground-water remediation technology. EPA/600/8-90/003, pp.66.

794 USEPA (1996). Pump-and-treat ground-water remediation: A guide for decision makers and practitioners.
795 EPA/625/R-95/005, pp. 91.

796 USEPA (1997). Design guidelines for conventional pump-and-treat systems. EPA/540/S-97/504.

USEPA (2021). Green remediation best management practices: Pump and treat systems. Office of Land and Emergency Management, EPA 542-F-21-029., pp 6.

van Breukelen, B. M. and Griffioen, J. (2004). Biogeochemical processes at the fringe of a landfill leachate pollution plume: Potential for dissolved organic carbon, Fe(II), Mn(II), $NH_4$, and $CH_4$ oxidation. J. Contaminant Hydrology, 73, 181−205.

van Leeuwen, J. A., Gerritse, J., Hartog, N., Ertl, S., Parsons, J. R. and Hassanizadeh, S. M. (2022). Anaerobic degradation of benzene and other aromatic hydrocarbons in a tar-derived plume: Nitrate versus iron reducing conditions. Journal of Contaminant Hydrology, 248, 104006.

Vencelides, Z., Sracek, O. and Prommer, H. (2007). Modelling of iron cycling and its impact on the electron balance at a petroleum hydrocarbon contaminated site in Hnevice, Czech Republic. Journal of Contaminant Hydrology, 89, 270-294. 10.1016/j.jconhyd.2006.09.003.

Watson, I. A., Oswald, S.E., Banwart, S.A., Crouch, R.S. and Thornton, S.F. (2005). Modeling the dynamics of fermentation and respiratory processes in a groundwater plume of phenolic contaminants interpreted from laboratory-to field-scale. Environmental Science and Technology 39, 8829-8839.

Werth, C. J., Cirpka, O. A. and Grathwohl, P. (2006). Enhanced mixing and reaction through flow focusing in heterogeneous porous media. Water Resources Research, 42, https://doi.org/10.1029/2005WR004511.

Wiedemeier, T. H., Rifai, H. S., C. Newell, C.J., and Wilson. J.T. (1999). Natural attenuation of fuels and chlorinated solvents in the subsurface. John Wiley & Sons

Williams, G. M., Pickup, R. W., Thornton, S. F., Lerner, D. N., Mallinson, H. E. H., Moore, Y. and White, C. (2001). Biogeochemical characterisation of a coal-tar distillate plume J. of Contaminant Hydrology, 53, 175-198.

Winderl, C., Anneser, B., Griebler, C., Meckenstock, R. U., and Lueders, T. (2008). Depth-resolved quantification of anaerobic toluene degraders and aquifer microbial community patterns in distinct redox zones of a tar oil contaminant plume. Applied Environmental Microbiology, 74,792−801.

Wu, Y., Lerner, D. N., Banwart, S. A., Thornton, S. F. and Pickup, R. W. (2006). Persistence of fermentative process to phenolic toxicity in ground water. J. Environmental Quality, 35, 2021-2025.

Xu, T., Ye, Y., Zhang, Y. and Xie, Y. (2018). Recent advances in experimental studies of steady-state dilution and reactive mixing in saturated porous media. Water, 11(1), 3 https://doi.org/10.3390/w11010003.

Xu, M. and Eckstein, Y. (1995). Use of weighted least-squares method in evaluation of the relationship between dispersivity and field scale. Groundwater, 33, 905-908.

Ye, Y., Chiogna, G., Cirpka, O. A., Grathwohl, P. and Rolle, M. (2015). Enhancement of plume dilution in two-dimensional and three-dimensional porous media by flow focusing in high-permeability inclusions. Water Resources Research, 51, doi:10.1002/2015WR016962.

Ye, Y., Zhang, Y., Lu, C., Xie, Y. and Luo, J. (2021). Effective chemical delivery through multi-screen wells to enhance mixing and reaction of solute plumes in porous media. Water Resources Research, 57, e2020WR028551. doi.org/10.1029/2020WR028551.

## Statements and Declarations

### Ethical Approval

Not applicable.

### Consent to Participate

Not applicable.

### Consent to Publish

All the authors give their permission to publish this research.

### Author Contributions

Luther M. Brown completed the research work for the publication, including model development and analysis, interpretation, and preparation of the publication.

Steven F. Thornton assisted with the conceptual model development and supervised the modelling work and contributed to data analysis and the writing of the paper, including reviews.

Domenico Baú supervised the modelling work and contributed to data analysis and the writing of the paper, including reviews.

### Funding

This research was completed while Luther Brown was completing a PhD at the University of Sheffield. The authors declare that no funds, grants, or other support were received during the preparation of this manuscript.

## Competing Interests

The authors confirm that there are no conflicts of interest.

**Table 1.** Input parameters used in the scenario modelling.

| **Flow and transport parameters** | | **Value** | | **Data source** |
|---|---|---|---|---|
| Effective porosity (-) | | 0.125[a] | | Core samples/geophysical logs[a] |
| Hydraulic conductivity range, K (m/d) | | 0.35-1.0[a] | | Pumping tests and RFM[c] |
| Recharge rate (m/d) | | 8.00e-04[a] | | Effective infiltration estimation[b] |
| Longitudinal dispersivity (m) | | 1[b] | | |
| Vertical transverse dispersivity (m) | | 4.00e-03[b] | | Tracer tests and numerical modelling |
| Horizontal transverse dispersivity (m) | | 1.00e-02[b] | | |
| Grid block size ($m^3$) | | 5 | | Well screen lengths are 5 meters.[a] |
| Model length, width, and depth (m) | | 1200x300x255 | | |
| | | **Species** | | |
| *Biodegradation module parameters* | *Phenol* | *Oxygen* | *Nitrate* | |
| Half saturation constant (mg/l) | - | 0.1[b] | 0.5[b] | Determined by a mesocosm experiment[b] |
| Inhibition constant (mg/l) | - | 0.9[b] | 0.9[b] | |
| Decay rate (1/T) | - | 3.44e-05[b] | 3.44e-06[b] | |
| Yield coefficient (-) | 0 | 2.38[b] | 3.69[b] | Reaction stoichiometry (Eq. 3) |
| Source concentration (mg/l) | 25000 | 0 | 0 | Groundwater quality monitoring |
| Background groundwater concentration (mg/l) | 0 | 4.5-9.28[b] | 91-105[b] | Groundwater quality monitoring |

a. Unpublished data from confidential third party consultant reports.
b. Values used in previous modelling studies on the site [Watson et al. (2005) and Mayer et al. (2001)].
c. RFM refers to Radial Flow Modelling undertaken by third party consultants.

**Table 2.** Scenarios (A-F) evaluated in 10-year modelling simulations and the respective approach followed (see text for explanation).

| Scenario | Description | Injection/extraction well layout |
|---|---|---|
| A. Effect of extraction well distance along flow path | Extraction well is located on the plume centerline, at distances which increase by 200m in successive simulations. Well extraction rate is fixed at $\underline{Q}$=30 m$^3$/d. | 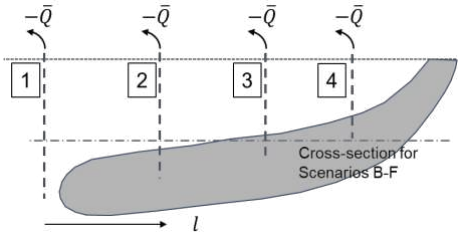  |
| B. Effect of asynchronous injection and extraction rate | Well location is fixed ($\underline{d}$=m) and injection/extraction rate $Q$ progressively increased. This scenario includes injection of either GWWEA or GW in separate sub-scenarios (see text). | 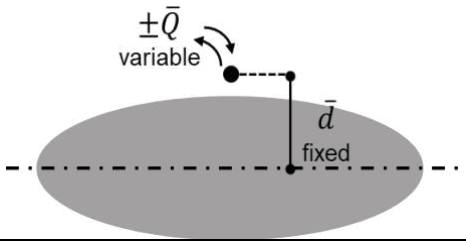  |
| C. Effect of asynchronous extraction/injection well location lateral to flow path | Injection/extraction well is moved an increasing lateral distance from the plume centerline. Well pumping rate is fixed at $\underline{Q}$=±30 m$^3$/d. This scenario includes injection of either GWWEA or GW in separate sub-scenarios (see text). | 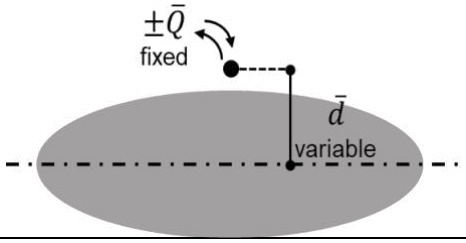  |
| D. Effect of well pumping rate for two concurrent extraction wells | Extraction wells are placed symmetrically at a fixed lateral distance $\underline{d}$=m from the plume centerline, with $\underline{Q}$ progressively increased. | 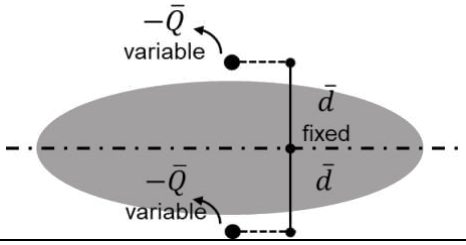  |
| E. Effect of location for two concurrent extraction wells | Extraction wells are placed symmetrically at a progressively increasing lateral distance $\underline{d}$ from the plume centerline, with $\underline{Q}$ fixed at 60 m$^3$/d. | 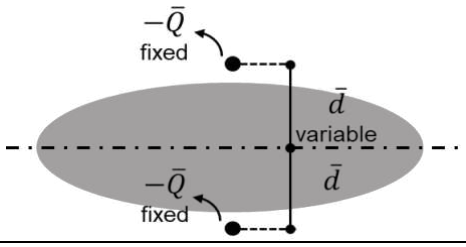  |
| F. Effect of location for concurrent extraction and injection wells | Injection well is located on the plume centerline and one extraction well is positioned laterally at an increasing distance $\underline{d}$, with the pumping rate $\underline{Q}$ fixed at ±30 m$^3$/d. This scenario includes injection of either GWWEA or GW in separate sub-scenarios (see text). | 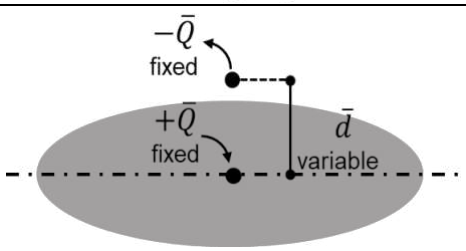  |

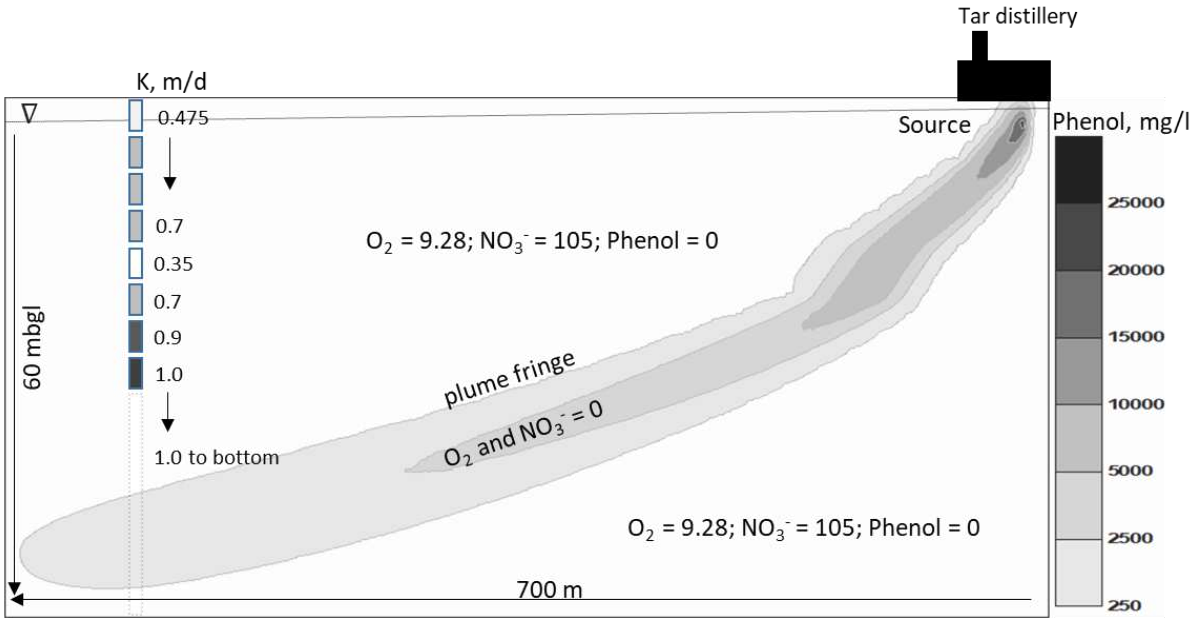


**Figure 1.** Schematic of plume concentration envelope based on groundwater chemistry and numerical simulation of site data. The concentrations shown are in mg/l. The hydraulic conductivity scale indicates that some values repeat throughout the layered system (Thornton et al., 2001b). Note that the concentrations of oxygen and nitrate are below detection in the plume due to biodegradation of the phenolic compounds. Note the vertical exaggeration of the depth scale.

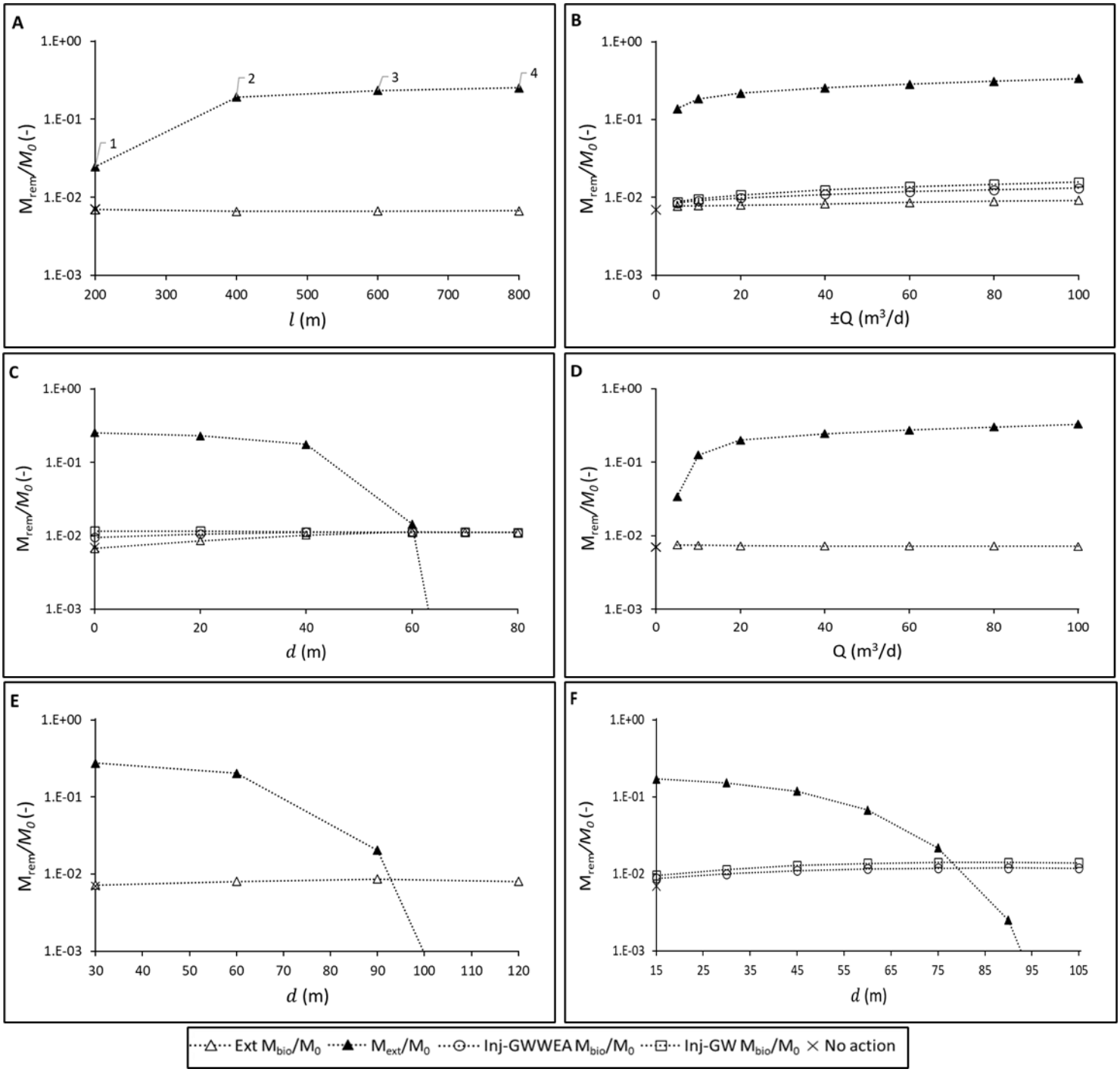


**Figure 2**. Ratios of contaminant mass removed for scenarios A-F. The y-axis is the contaminant mass removed ($M_{rem}$) by biodegradation *in situ* ($M_{bio}$) and extraction ($M_{ext}$), normalised to the initial mass ($M_0$). For Scenario A, the numbered points correspond to the well locations in Table 2, where well 1 is at the front of the plume (200m), downgradient of the source, and well 4 is close to the source (800m). "No action" refers to the initial condition in which NA occurs without PAT intervention.

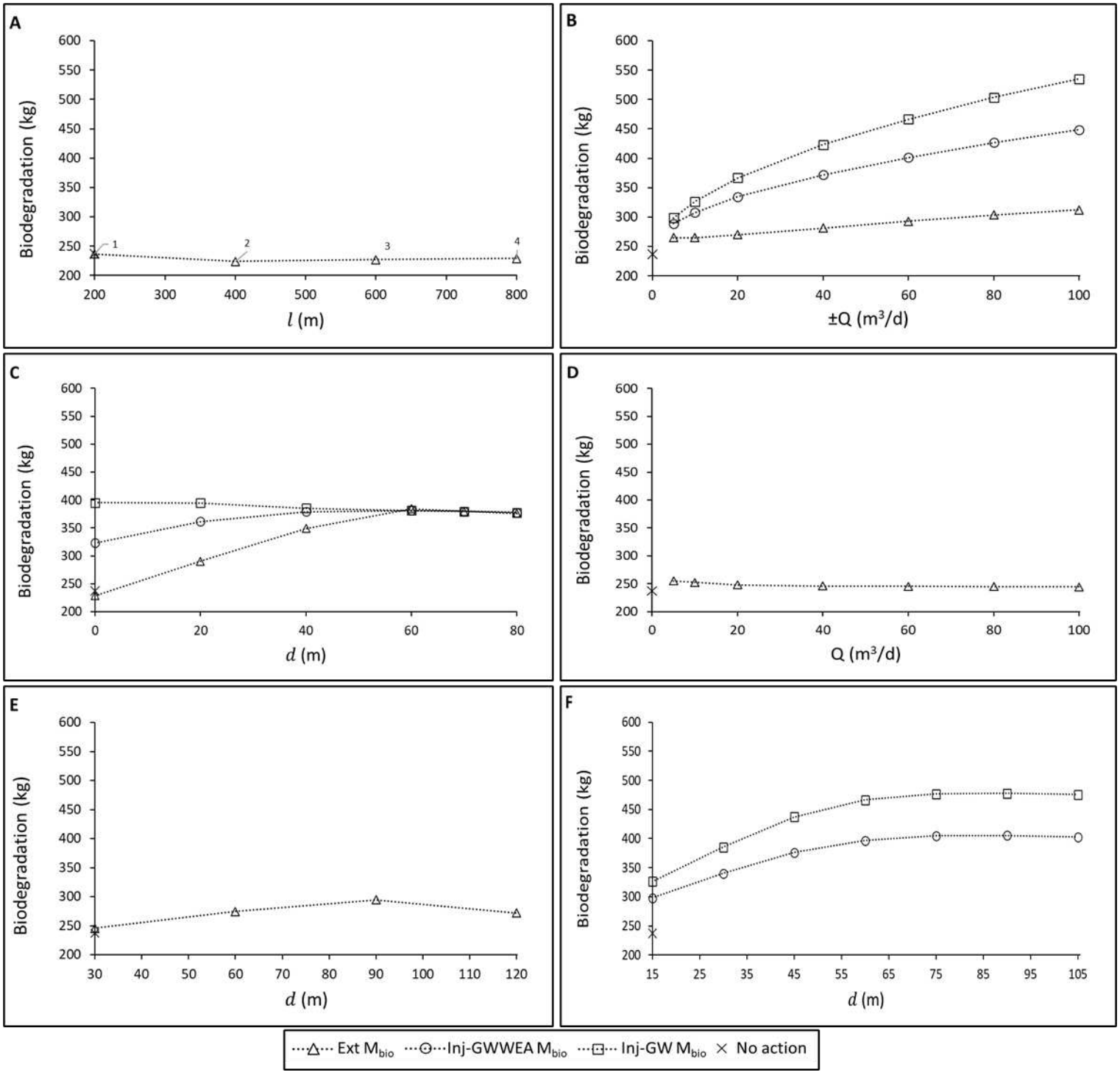


**Figure 3.** Mass removed by biodegradation for scenarios A-F. The x-axis is the variable under consideration for the particular scenario and the y-axis is the mass removed by biodegradation, for the entire model domain over 10 years, in kilograms. GWWEA is injection of groundwater without EAs and GW is injection of groundwater with EAs.

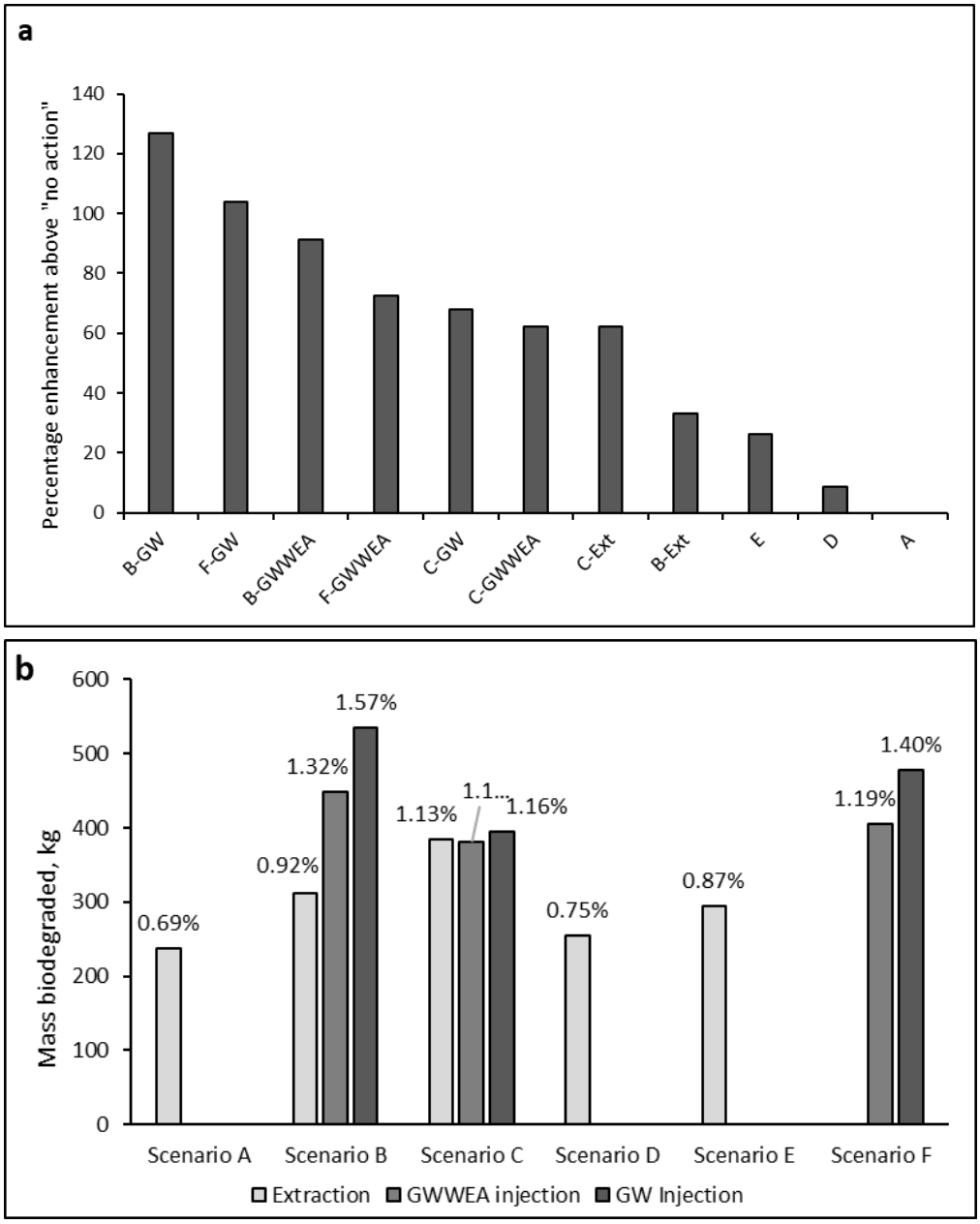


**Figure 4.** (a) Scenarios with respective sub-scenarios ranked by percentage enhancement in biodegradation above "no action", from highest to lowest. (b) Absolute and percentage of total plume mass biodegraded.

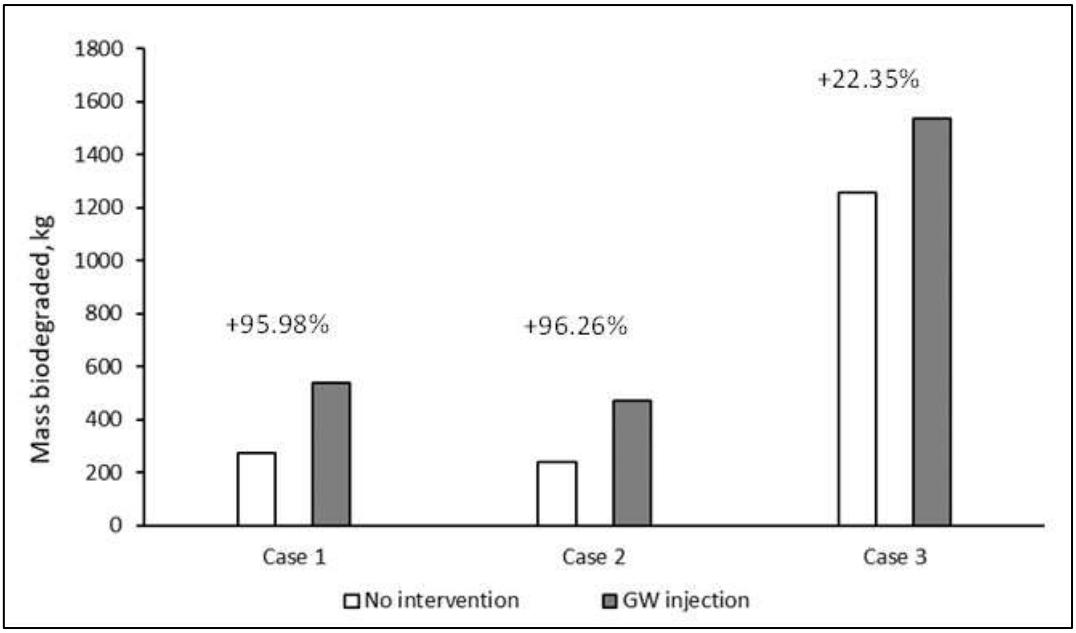


**Figure 5.** Total mass removed by biodegradation for an experiment in which the dispersivity in all dimensions is changed for three test cases, each of which were simulated over 10 years. Each test case is split into a simulation with "no action", in which there are no wells and only intrinsic biodegradation is measured, and a simulation with groundwater injection at 30 $m^3$/d with a well located 15m lateral to the plume centerline (same location as Scenario B-GW). In case 1, the dispersivity is the same as the baseline model ($\alpha_x$=1m, $\alpha_y$=1e-2m, $\alpha_z$=4e-3m). In case 2, the dispersivity is reduced 10x from case 1 ($\alpha_x$=0.1m, $\alpha_y$=1e-3m, $\alpha_z$=4e-4m) and in case 3, the dispersivity is increased 10x from case 1 ($\alpha_x$=10m, $\alpha_y$=1e-1m, $\alpha_z$=4e-2m). The percentages show the enhancement of biodegradation above the "no action" case due to GW injection.

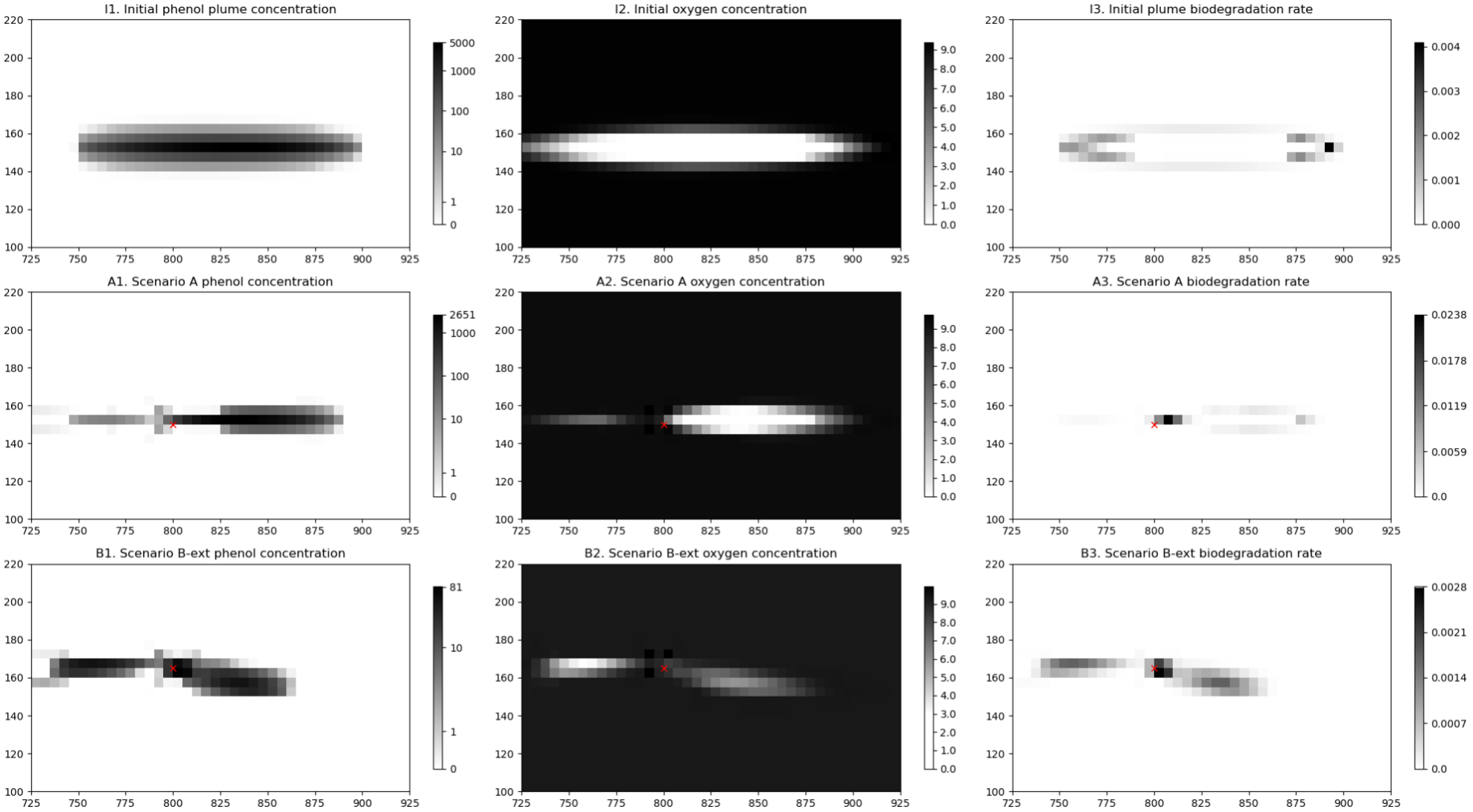
I1. Initial phenol plume concentration
I2. Initial oxygen concentration
I3. Initial plume biodegradation rate
A1. Scenario A phenol concentration
A2. Scenario A oxygen concentration
A3. Scenario A biodegradation rate
B1. Scenario B-ext phenol concentration
B2. Scenario B-ext oxygen concentration
B3. Scenario B-ext biodegradation rate

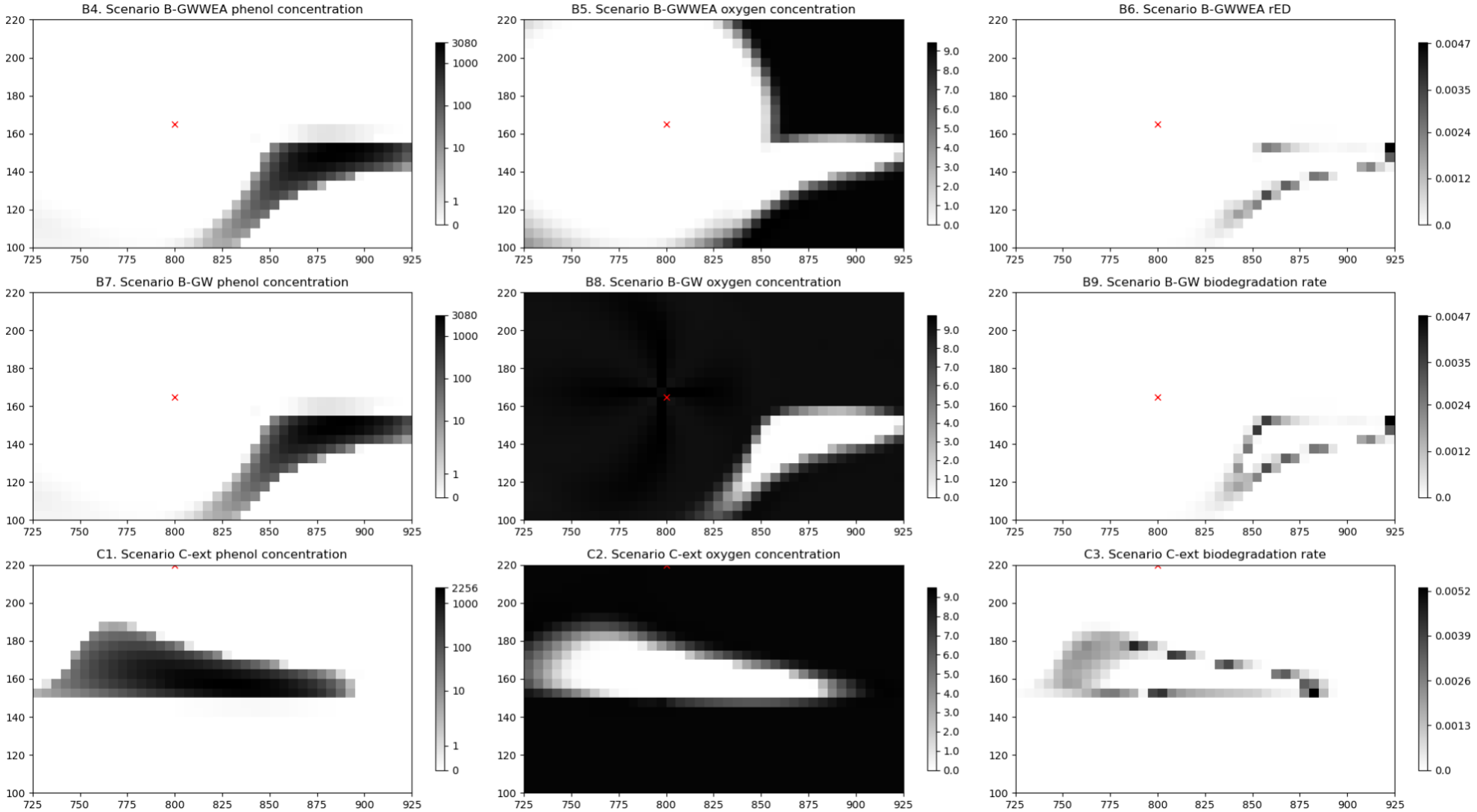
B4. Scenario B-GWWEA phenol concentration
B5. Scenario B-GWWEA oxygen concentration
B6. Scenario B-GWWEA rED
B7. Scenario B-GW phenol concentration
B8. Scenario B-GW oxygen concentration
B9. Scenario B-GW biodegradation rate
C1. Scenario C-ext phenol concentration
C2. Scenario C-ext oxygen concentration
C3. Scenario C-ext biodegradation rate

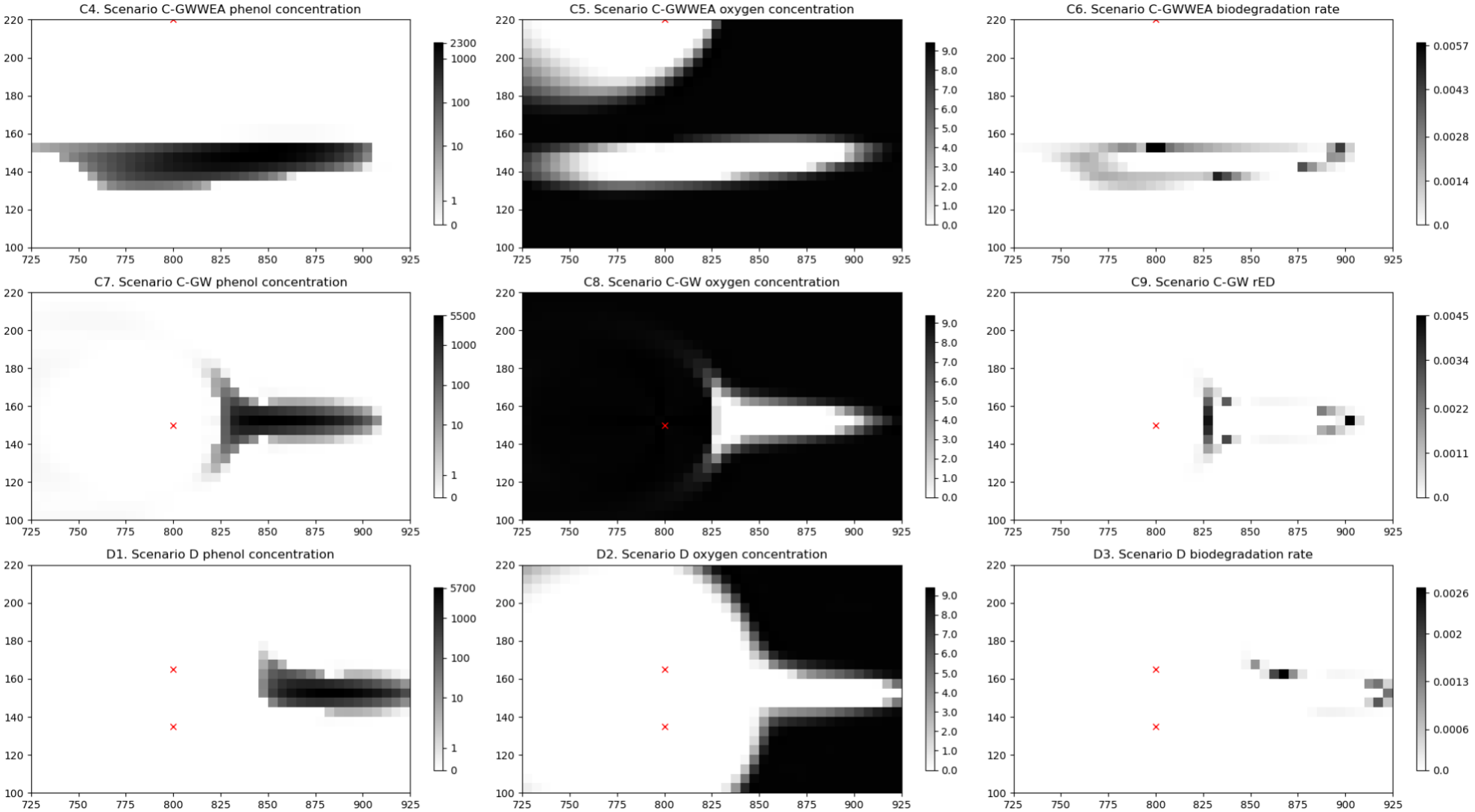
C4. Scenario C-GWWEA phenol concentration
C5. Scenario C-GWWEA oxygen concentration
C6. Scenario C-GWWEA biodegradation rate
C7. Scenario C-GW phenol concentration
C8. Scenario C-GW oxygen concentration
C9. Scenario C-GW rED
D1. Scenario D phenol concentration
D2. Scenario D oxygen concentration
D3. Scenario D biodegradation rate

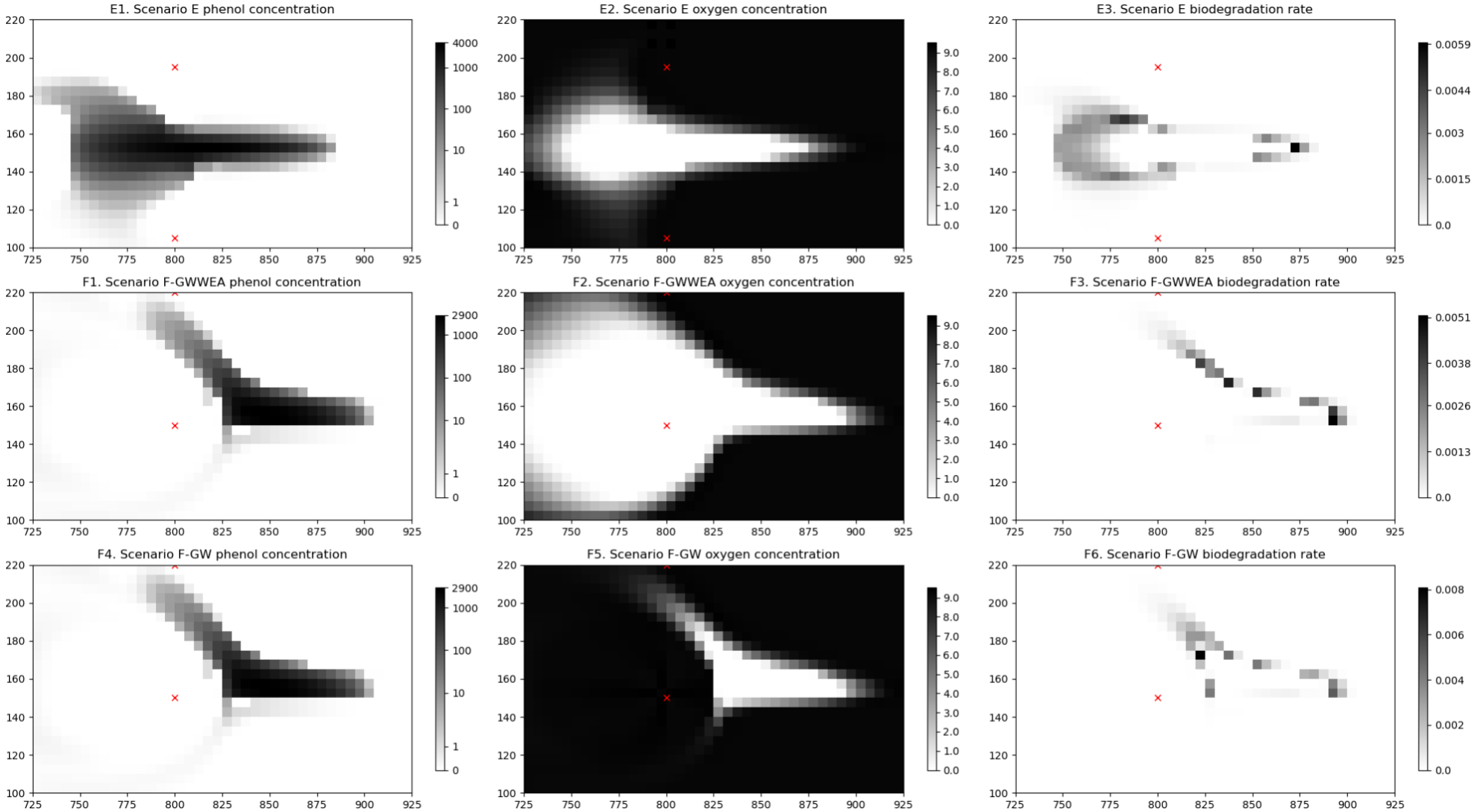


**Figure S1.** Pixelized concentrations of phenol, oxygen and the biodegradation rate (rED) for each modelling scenario. Concentrations are in units of mg/l and rED is in units of mg/l/d. Each graph is produced at the end of 10 years. For brevity, only the most effective scenario data points have been presented and only 1 layer of the results are shown. For Scenario A, only the simulation at 800m is shown. For Scenario B-Ext, only the simulation at -100 $m^3$/d is shown. For Scenario C-GW, the most effective simulation is shown, with the injection well at the center of the plume. The red 'x' indicates the location of pumping well(s). The phenol concentrations (left panel) are shown on a symmetrical logarithmic scale, whereas the other graphs are shown on a linear scale.